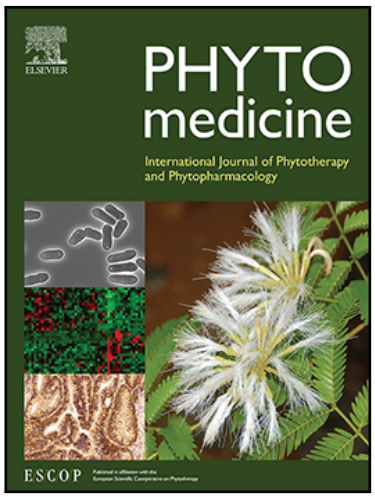

Targeting the smooth muscle cell KEAP1-Nrf2-STING axis with pterostilbene attenuates abdominal aortic aneurysm

Jiami Zou , Zhihua Zheng , Weile Ye , Mei Jin , Pinglian Yang , Peter J Little , Jiaojiao Wang , Zhiping Liu

PII: S0944-7113(24)00355-6
DOI: https://doi.org/10.1016/j.phymed.2024.155696
Reference: PHYMED 155696

To appear in: *Phytomedicine*

Received date: 21 December 2023
Revised date: 27 April 2024
Accepted date: 29 April 2024

Please cite this article as: Jiami Zou , Zhihua Zheng , Weile Ye , Mei Jin , Pinglian Yang , Peter J Little , Jiaojiao Wang , Zhiping Liu , Targeting the smooth muscle cell KEAP1-Nrf2-STING axis with pterostilbene attenuates abdominal aortic aneurysm, *Phytomedicine* (2024), doi: https://doi.org/10.1016/j.phymed.2024.155696

Targeting the smooth muscle cell KEAP1-Nrf2-STING axis with pterostilbene attenuates abdominal aortic aneurysm

Jiami Zou[a,1], Zhihua Zheng[a,1], Weile Ye[a,1], Mei Jin[a], Pinglian Yang[a], Peter J Little[b,c], Jiaojiao Wang[d,*], Zhiping Liu[a,*]

[a] State Key Laboratory of Bioactive Molecules and Druggability Assessment, Guangdong Province Key Laboratory of Pharmacodynamic Constituents of TCM and New Drugs Research, International Cooperative Laboratory of Traditional Chinese Medicine Modernization and Innovative Drug Discovery of Chinese Ministry of Education (MOE), College of Pharmacy, Jinan University, Guangzhou 510632, China.

[b] School of Pharmacy, Pharmacy Australia Centre of Excellence, The University of Queensland, Woolloongabba, QLD 4102, Australia.

[c] Department of Pharmacy, Guangzhou Xinhua University, Guangzhou, 510520, China.

[d] Key Laboratory of Big Data Mining and Precision Drug Design of Guangdong Medical University, Key Laboratory for Research and Development of Natural Drugs of Guangdong Province, School of Pharmacy, Guangdong Medical University, Dongguan, Guangdong, 523808, China

[1]These authors contributed equally.

*** To whom correspondence should be addressed:**

Zhiping Liu, PhD,

College of Pharmacy, Jinan University, No. 855, East Xingye Avenue, 511436, Guangzhou, China. E-mail: liuzhiping@jnu.edu.cn, Tel.: +86-13527620210, Fax: 020-37331255

Jiaojiao Wang, PhD,

School of Pharmacy, Guangdong Medical University, No. 1 Xincheng Road, Dongguan, Guangdong Province, 523808, China. E-mail: jjwang89@163.com, Tel.:

+86-13450267392, Fax: 0769-22896557

Abbreviations: AAA, abdominal aortic aneurysm; AAV, adeno-associated virus; Ang II, angiotensin II; ARE, antioxidant response elements; $ApoE^{-/-}$, apolipoprotein E-deficient; CVDs, cardiovascular diseases; Ccl2, monocyte chemoattractant protein-1; CD68, cluster of differentiation 68; CCK-8, cell counting kit-8; CETSA, cellular thermal shift assay; CNN1, calponin 1; cGAMP, cyclic guanosine monophosphate-adenosine monophosphate; cfDNA, cytosolic-free DNA; DAB, diaminobenzidine; DAPI, 4′,6-diamidino-2-phenylindole; DHE, dihydroethidium; DMSO, dimethyl sulfoxide; D-Loop, displacement loop region; Doxy, doxycycline; dsDNA, double-stranded deoxyribonucleic acid; DMEM, dulbecco's modified eagle's medium; DRP1, dynamin-related protein 1; eNOS, endothelial nitric oxide synthase； EVG, elastin van gieson; ECM, extracellular matrix; VCAM-1, vascular cell adhesion molecule 1; FBS, fetal bovine serum; GCLM, glutamate-cysteine ligase, modifier subunit; GFP, green fluorescent protein; HBSS, Hank's Balanced Salt Solution; H&E, hematoxylin and eosin; HO-1, heme oxygenase 1; Il1b, interleukin-1 beta; ICAM-1, intercellular adhesion molecule 1; IRF3, interferon regulatory factor 3; ITDRF, isothermal dose-response fingerprint; KEAP1, kelch-like ECH-associated protein 1; MASMCs, mouse aortic smooth muscle cells; MMP, matrix metalloproteinases; MFN2, mitofusin2; mtDNA, mitochondrial DNA; Nd1, NADH dehydrogenase 1; NF-κB; nuclear factor kappa-light-chain-enhancer of activated B cells; NQO1, NAD(P)H quinone dehydrogenase 1; Nrf2, nuclear factor erythroid 2-related factor 2; PBS, phosphate buffer solution; Pt, pterostilbene; RASMCs, rat aortic smooth muscle cells; RNA-seq, RNA sequencing; ROS, reactive oxygen species; qPCR, quantitative polymerase chain reaction; shRNA, small short hairpin RNA; SEM, standard error of mean; SM22α, smooth muscle 22α; STING, stimulator of interferon genes; TBHQ, tertiary butylhydroquinone; TBK1, tank-binding kinase 1; TNF-α, tumor necrosis factor-α; VE-cadherin, vascular endothelial-cadherin; VSMCs, vascular smooth muscle cells; VDAC1, voltage dependent anion channel 1; WB, western blot; α-SMA, α-smooth muscle actin; 18s rRNA, 18s ribosomal RNA.

ABSTRACT

Background: Abdominal aortic aneurysm (AAA) is a life-threatening aortic disease, and to date, there are currently no effective pharmacological treatments to address this condition. Activation of cytosolic DNA sensing adaptor stimulator of interferon genes (STING) signaling is a crucial mechanism in AAA formation.

Purpose: This study investigated pterostilbene (Pt), a naturally occurring polyphenol and resveratrol analogue, as a STING inhibitor for preventing AAA.

Methods: We evaluated the effect of Pt on AAA formation in angiotensin II (AngII)-infused apolipoprotein E-deficient ($ApoE^{-/-}$) mice. We used histological analysis, MMP activity measurement, western blot, and immunohistochemistry to detect AAA formation and development. We applied RNA sequencing, molecular docking, cellular thermal shift assay (CETSA) and functional studies to dissect the molecular mechanism of Pt-regulating KEAP1-Nrf2-STING signaling. We conditionally knocked down Nrf2 in vascular smooth muscle cells (VSMCs) *in vivo* to investigate its role in Pt-mediated protective effects on AAA.

Results: Pt effectively blocked the formation of AAA in AngII-infused $ApoE^{-/-}$ mice. Whole transcriptome sequencing analysis revealed that nuclear factor erythroid 2-related factor 2 (Nrf2) and STING pathway in VSMCs were linked to the anti-AAA effects of pterostilbene. Mechanistically, Pt upregulated Nrf2 target genes (e.g., HO-1 and NQO1) through activation of the KEAP1/Nrf2 signaling, which restricted the immunostimulatory axis of mtDNA-STING-TBK1-NF-κB, thereby alleviating VSMC inflammation and preserving the VSMC contractile phenotype. Subsequently, molecular docking and CETSA revealed a binding mode between Pt and KEAP1/Nrf2. Intriguingly, the inhibitory effect of Pt on STING signaling and the protective role of Pt in AAA were largely abrogated by VSMC-specific Nrf2 knockdown in mice.

Conclusion: Collectively, naturally derived Pt shows promising efficacy for the treatment of AAA by targeting the KEAP1-Nrf2-STING axis in VSMCs.

Keywords: Pterostilbene; Abdominal Aortic Aneurysm; mtDNA; STING; Nrf2; Smooth Muscle Cell

Introduction

Abdominal aortic aneurysm (AAA) is a severe vascular condition which may rupture spontaneously and it is associated with a high mortality rate (Bossone and Eagle, 2021; Golledge, 2019). Pathological features of AAA include degeneration of the elastic lamina within the lamellae aorta, overproduction of reactive oxygen species (ROS), high levels of matrix metalloproteinases (MMPs), malfunction of vascular smooth muscle cells (VSMCs), and chronic aortic wall inflammation (Golledge, 2019; Lu et al., 2020; Zhang et al., 2020). AAAs have a mortality rate of 85 to 90 percent when they rupture, despite patients being asymptomatic before the rupture event (Sakalihasan et al., 2005). At present, the only effective treatment is mechanical intervention, vascular support, which is however associated with significant perioperative mortality and morbidity (Buck et al., 2014; Zettervall et al., 2017). Furthermore, surgical intervention is not ideal for small aneurysms or aneurysms with anatomical limitations (Galyfos et al., 2020; Sakalihasan et al., 2005). Therefore, efficacious pharmaceutical interventions capable of reducing the pathological progression of AAA and limiting the propensity to vessel rupture are much needed additions to the therapeutic options in this area of vascular medicine.

Naturally occurring compounds, especially polyphenols, hold promise in creating new treatments for cardiovascular diseases (CVDs), mostly associated with their multiple bioactive properties relevant to inhibition of tissue inflammation and redox disturbances (Behl et al., 2020; Kim et al., 2014). Pterostilbene (Pt, Fig. 1A), a polyphenolic compound that occurs naturally in blueberries and various grape varieties, is widely acknowledged for its pharmacological benefits, encompassing anti-inflammatory (Xu et al., 2023), anti-oxidant, and anti-apoptotic activities (Liu et al., 2017). The available evidence indicates that Pt may be beneficial in the treatment of CVDs, including atherosclerosis, restenosis after angioplasty, and hypertension (Park et al., 2010; Zhang and Zhang, 2016). These results have led to our interest in

exploring the potential therapeutic role of Pt in the treatment and prevention of AAA and its clinical consequences.

Our current study identified that Pt suppressed AAA formation in Ang II-induced ApoE$^{-/-}$ mice. Whole transcriptome sequencing analysis revealed that the KEAP1/Nuclear factor erythroid 2-related factor 2 (Nrf2) pathway in VSMCs was a principal target associated with the anti-AAA effect of Pt. Under physiological circumstances, KEAP1 attaches to the transcription factor Nrf2 in the cytoplasm, resulting in Nrf2 ubiquitination and degradation. Under oxidative stress, Nrf2 translocates to the nucleus and interacts with antioxidant response elements, initiating the transcription of downstream targets such as heme oxygenase 1 (HMOX1, also known as HO-1) (Yamamoto et al., 2018). Importantly, previous research has demonstrated that activation of the Nrf2 pathway and its downstream effector proteins, particularly HO-1, prevents AAA formation by preserving cellular oxidative stress homeostasis and attenuating inflammation (Ho et al., 2016; Song et al., 2020). ROS detoxification is enhanced by activation of Nrf2, and elimination of ROS is thought to be the molecular foundation of Nrf2-mediated anti-inflammation (Kobayashi et al., 2016; Thimmulappa et al., 2006). Furthermore, ROS induces mitochondrial damage and subsequent release of cytosolic mitochondrial DNA (mtDNA), which activates the cytosolic DNA sensing adaptor, stimulator of interferon genes (STING, also known as TMEM173) (Mohamed et al., 2020; Olagnier et al., 2018). As a regulator of the innate immune response, STING activates downstream TBK1/IRF3-NF-κB signaling to participate in tissue inflammation. The aberrant activation of STING contributes to aortic aneurysm and dissection by inducing the inflammatory response, the DNA damage response, matrix metalloproteinase (MMP) production, and cell death in VSMCs (Luo et al., 2020; Oduro et al., 2022). As a downstream effector of STING, the NF-κB family plays an essential part in the regulation of inflammatory genes (Hayden and Ghosh, 2008). Based on these data, we postulated that Pt might inhibit AAA formation by negatively modulating the mtDNA-STING-NF-κB pathway via activation of Nrf2 and its

downstream target genes. To further investigate the pivotal role of Nrf2 activation in VSMCs and the protective effect of Pt against AAA, we generated SMC-specific Nrf2-knockdown mice using an adeno-associated viral vector (AAV) and found that SMC-specific Nrf2 knockdown significantly diminishes the protective effect of Pt on AAA. Collectively, our findings demonstrate that Pt targets the VSMC-specific KEAP1-Nrf2-STING axis to restrict AAA formation.

2. Materials and methods

2.1 Animals experiment

All experiments were performed with 12-week-old male apolipoprotein E-deficient ($ApoE^{-/-}$) mice acquired from Gempharmatech Company (Guangdong, China). Alzet osmotic minipumps (model 2004) containing Ang II (Enzo, 1,000 ng/kg/min) or saline (0.9% NaCl) were subcutaneously implanted in the $ApoE^{-/-}$ mice for 28 days. AAA was defined as being present when the maximal aortic diameter was 50% larger than its adjacent region. Animal Research Committee approved all animal research (Approval No. IACUC-20230625-11), and it was carried out in line with the Chinese Animal Welfare Law.

After an acclimatization period of one week, male $ApoE^{-/-}$ mice were randomly allocated into four experimental groups: the Saline group, the Ang II group, the Pt-Low (L) + Ang II group, and the Pt-High (H) + Ang II group. Apart from the Saline group, the other three groups of $ApoE^{-/-}$ mice were infused with Ang II (1,000 ng/kg/min) for 28 days (Fig. 1B). On postoperative day 2, the Pt-L + Ang II and the Pt-H + Ang II groups received daily gavage of Pt (15 mg/kg/day (L) or 30 mg/kg/day (H)) for 27 consecutive days.

Small short hairpin RNA (shRNA) targeting Nrf2 was cloned and packaged into an adeno-associated viral (AAV) serotype 2 vector carrying the SMC-specific SM22α promoter to achieve SMC-specific knockdown of Nrf2 in mice. We acquired all recombinant viruses from Vigene Biosciences Company Limited (China). AAV

vectors containing the shNrf2 coding sequence (CTTGAAGTCTTCAGCATGTTA) along with GFP, as well as control viruses carrying only GFP, were administered through tail vein injections into $ApoE^{-/-}$ mice. Each mouse received a dose of 5×10^{11} vector genomes (vg). Two weeks post-injection, the murine AAA model was established and the mice were subsequently treated with 0.5% CMC-Na or a high dose of Pt (Fig. 7B).

2.2 Reagents and antibodies

Pt ($C_{16}H_{16}O_3$; > 98% pure; B21702; S26817) and Doxycycline (B27273) were sourced from Shanghai Yuanye Biotechnology Company (Shanghai, China). Angiotensin II (ALX-151-039-M025) was obtained from Enzo Life Sciences (Ramsdonksveer, The Netherlands). ALZET® osmotic pumps (model 2004) were from Durect Corporation (Cupertino, CA). TNF-α (300-01A) was from Peprotech (NJ, USA). Cell Counting Kit-8 (CCK-8-100) was from GBCBIO Biotechnology Company (Guangzhou, China). Collagenase II (LS004176), elastase (2279), and soybean trypsin inhibitor (3571) were purchased from Worthington Biochemical (USA), and Hank's Balanced Salt Solution (HBSS, 24020) was purchased from Gibco (Grand Island, NY). ML385 (846557-71-9) was purchased from Target Molecule Corporation (Shanghai, China). TBHQ (HY-100489) was provided by MedChemExpress (New Jersey, USA). Antibodies against Tom20 (FL-145), MMP-2 (sc-13595), GCLM (sc-55586), NQO1 (sc-32793), and VE-cadherin (sc-9989) were purchased from Santa Cruz Biotechnology (California). Antibodies against GAPDH (60004-1-Ig), α-Tubulin (11224-1-AP), MFN2 (12186-1-AP), VDAC1 (55259-1-AP), DRP1 (12957-1-AP), and Nrf2 (16396-1-AP) were purchased from Proteintech Group (IL, USA). Antibodies against HO-1 (R24541), KEAP1 (R26935), MMP3 (12163S), MMP-9 (502095), VCAM-1 (383318), ICAM-1 (384650), α-SMA (380653), and Lamin B1 (R24825) were obtained from ZENBIO (Chengdu, China). Antibodies against STING (13647), p-STING (72971), p-TBK1 (5483), and p-P65 (3033) were obtained from Cell Signaling Technology (Arundel, Australia). MMP-9 (ab38898) and

dsDNA (ab27156) were purchased from Abcam (Cambridge, MA, USA). Antibody p-IRF3 (Ser396) (AF2436) was purchased from Affinity Biosciences (China). The Nuclear and Cytoplasmic Protein Extraction Kit (P0028) and antibodies against p65 (AN365) and β-Actin (AF0003) were obtained from Beyotime Biotechnology (Shanghai, China). Antibodies against p-eNOS (PA5-104858) were purchased from Thermo (Massachusetts, USA).

2.3 Histological analysis

Tissue sections were prepared from paraffin-embedded aortas and stained with hematoxylin and eosin (H&E) for general morphology, Elastin van Gieson (EVG) for detecting elastin integrity, and Masson's Trichrome for visualizing collagen content. Elastin degradation was quantified by counting the number of breaks per vessel in the stained sections.

2.4 Immunohistochemistry staining

For immunohistochemistry, after deparaffinization, rehydration, and antigen retrieval, paraffin-embedded sections were incubated with primary antibodies and appropriate biotin-conjugated secondary antibodies. A 3,3’-diaminobenzidine (DAB) peroxidase substrate kit (SK4100; Vector Labs, USA) was used to visualize positive antibody binding. Hematoxylin was used to stain nuclei and a microscope (BX53; OLYMPUS) was used to capture bright-field images.

2.5 Molecular docking analysis

The structure of Pt (Compound CID: 5281727) was obtained from the PubChem database (https://pubchem.ncbi.nlm.nih.gov/). The KEAP1 protein’s crystal structure (PDB code: 1U6D) was acquired from the RCSB Protein Data Bank (https://www.rcsb.org/). The molecular docking model of Pt with KEAP1 was carried out by Molecular Operating Environment 2015 (MOE 2015, Chemical Computing Group ULC). Subsequently, hydrogen atoms were incorporated into the KEAP1 protein structure, and water molecules were removed. Compound Pt was positioned

throughout the molecular docking process. Following molecular docking, the interactions between KEAP1 and Pt were analyzed to understand their binding dynamics.

2.6 Cell isolation, culture and treatments

Rat aortic smooth muscle cells (RASMCs) were extracted from the rat abdominal aorta. In brief, the rat abdominal aorta was isolated and rinsed in a cold phosphate buffer solution (PBS). After the endothelium and adventitia were removed, the aorta was sliced into 1-2 mm fragments and placed onto cell culture dishes. Cells were released from the vessel fragments and proliferation was allowed to continue until the cells achieved confluence. Cells were cultured in Dulbecco's modified Eagle's medium (DMEM, CR-12800) with the addition of 10% fetal bovine serum (AB-FBS-1050S) in a 5% CO_2 incubator at 37 °C with controlled humidity. After the identification of RASMCs by morphology and immunofluorescence, the 3-8-passage cells were used for experiments.

Mouse aortic smooth muscle cells (MASMCs) were isolated from 3 to 6-week-old mice as we previously described (Ma et al., 2022). Briefly, after CO_2-induced euthanasia, the aortas were excised following sterile PBS perfusion. Excess connective tissue was trimmed, and aortas were immersed in HBSS with 1 mg/mL collagenase II, 0.744 units/mL elastase, and 1 mg/mL soybean trypsin inhibitor, and incubated at 37°C in 5% CO_2 for 8 minutes. Adventitia was removed, endothelial cells were stripped using forceps, and the medial layers were further digested with the enzyme solution for one hour under the same conditions. The resultant MASMCs were cultured in DMEM with 10% FBS. Cells between the 3rd and 6th passages were used for experiments.

In some experiments, cells were pre-treated with different concentrations of Pt, 10 μM TBHQ, 50 μM Doxycycline, and 10 μM H151 for 2 hours, followed by stimulation with 10 ng/mL TNF-α for either 24 hours for protein extraction or 6 hours for RNA isolation. In the experiments utilizing a specific Nrf2 inhibitor, cells were

pre-treated with 1 μM ML385 for 1 hour, then 10 μM Pt and positive control drugs were added to the medium. 2 hours post ML385 pre-treatment, 10 ng/mL of TNF-α were added to the medium.

2.7 Cellular thermal shift assay (CETSA)

RASMCs were washed and partitioned into eight equal aliquots and heated at various temperatures ranging from 37 °C to 72 °C for 3 minutes, then cooled at ambient temperature for 2 minutes. Samples were freeze-thawed twice, mixed with loading buffer, and analyzed by WB.

To perform the ITDFR-CETSA experiment, RASMCs were treated by Pt in a dose-dependent manner (from 0 to 102.4 μM). Cells were collected and heated at 55 °C for 3 minutes, followed by 2 minutes of cooling. Protein samples were sufficiently lysed, and protein levels were measured by WB analysis.

2.8 RNA-seq analysis

RNA isolation was performed on RASMCs that were pre-treated with 10 μM Pt for 2 hours and then stimulated with TNF-α for 6 hours (n = 4 for each group) using the Trizol protocol, and 1-2 μg of RNA was utilized for whole transcriptome RNA-seq analysis. RNA-sequencing analysis was performed by the Omicsmart high-throughput sequencing service (Guangzhou, China). P-value adjustment was done using the false discovery rate method of Benjamini and Hochberg (R package DESeq2). Fold-change differences in mRNA expression level were visualized in a volcano plot, GO enrichment analysis, and KEGG pathway analysis using the OmicShare Platform with sample clustering.

2.9 Quantitative PCR

RASMCs were pre-treated with Pt (10 μM) for 2 hours and then stimulated with TNF-α for 6 hours. Cellular RNA was isolated following the manufacturer's guidelines using TRIzol reagent (15596018, Invitrogen). First-strand cDNA was produced utilizing First-Strand Synthesis Master Mix (F0202, LABLEAD) from 1 μg

of total RNA. The quantification of mRNA expression was performed using real-time PCR with SYBR Premix Ex Taq™ (Takara) on a LightCycler® 480 real-time PCR system (Roche). *Gapdh* and *Actb* were used as housekeeping genes. Relative expression was calculated using the $2^{-\Delta\Delta Ct}$ method. Primer sequences are detailed in Supplemental Table 1.

2.10 Western blot (WB) analysis

The adventitia and endothelium of the aorta of test mice were completely removed prior to tissue lysis. Mouse abdominal aortic tissue and cultured cells with equal amounts of total protein were separated by SDS-PAGE and transferred to 0.22 μm polyvinylidene fluoride membranes. Membranes were blocked with 5% nonfat milk and then incubated overnight at 4 °C with primary antibodies. Membranes were washed with TBST, incubated with the appropriate secondary antibody for 1 hour at room temperature and washed again. Protein band detection was performed on a Tanon 5200 chemiluminescent imaging system.

Nuclear and cytoplasmic protein lysates were extracted from VSMCs using the Nuclear and Cytoplasmic Protein Extraction Kit in accordance with the manufacturer's instructions.

2.11 Immunofluorescent staining

After three washes with cold PBS, RASMCs were fixed for 30 minutes with 4% paraformaldehyde. Cells were permeabilized for 45 minutes with 0.3% TritonX-100, blocked with 10% goat serum for 1.5 hours at room temperature, and then incubated with primary antibodies. Following PBS washing, the cells were incubated with an Alexa Fluor-conjugated secondary antibody (A23220, Abbkine) in a light-restricted environment at room temperature for 45 minutes. Ultimately, the nuclei were dyed with a DAPI solution for 15 minutes and the pictures were acquired using a laser confocal fluorescence microscope (Olympus, Tokyo, Japan).

2.12 Cell viability assay

Cells were cultured overnight in a 96-well plate at a density of 5×10^3 cells per well and then treated with various concentrations of Pt for 24 hours. Cell viability was evaluated using a CCK-8 kit, following the directions provided by the manufacturer.

2.13 ROS detection

RASMCs were incubated with 5 μM Dihydroethidium (DHE), a specific probe for superoxide anion ($\cdot O_2^-$) (Zhang et al., 2022b), at 37 °C for 30 minutes. The cells were rinsed with PBS to remove the unreacted DHE, digested with 0.05% trypsin, and suspended in cold PBS. ROS-positive cells were quantified and examined using a flow cytometer (BD FACScanto, Becton Dickinson), and data were analyzed using FlowJo software (BD Biosciences). Aortic tissue sections were also stained with 5 μM DHE at 37 °C for 30 minutes. ROS was identified by fluorescence microscopy using a Zeiss microscope.

2.14 Measurement of cytosolic dsDNA concentration and mtDNA

Cells were resuspended in 150 μL of digitonin lysis buffer (150 mM NaCl, 50 mM HEPES at pH 7.4, 25 μg/mL Digitonin). Suspension was placed on a rotator and incubated at 4 °C for 10 minutes. Lysates were centrifuged at 2,000 ×g. Supernatants were moved to a fresh tube and centrifuged at 20,000 ×g for 20 minutes. This process was repeated three times. The final supernatant, which contained cytosolic DNA, was moved to a fresh tube, while the pellet that contained mitochondria was discarded. The concentration of cytosolic DNA was measured using a Picogreen dsDNA Quantitation Reagent (12641ES01, Yeasen) following the directions provided by the manufacturer.

The initial pellet from the first centrifugation was washed with PBS. Pellet was resuspended into 150 μL NP-40 lysis buffer (150 mM NaCl, 50 mM HEPES pH 7.4, 1% NP-40) and incubated on ice for 30 minutes. The lysate was centrifuged at 7,000 ×g for 10 minutes at 4°C. Crude mitochondrial fraction in the supernatant and nuclear fraction in pellet were subsequently extracted using the Hipure Tissue DNA Mini Kit

(MAGEN). The mitochondrial DNA and ribosomal DNA were detected by quantitative polymerase chain reaction (qPCR) using corresponding primers, including NADH dehydrogenase 1 (*mt-Nd1*), displacement loop region (*D-Loop*), and 18s ribosomal DNA (*18s rRNA*) (Li et al., 2023).

2.15 MMP activity determined by *In Situ* zymography and gelatin zymography

Fluorescein-conjugated gelatin substrate DQ gelatin (D12054, Invitrogen) was used following the manufacturer's instructions. The diluted substrates were applied to aorta sections and incubated overnight. Fluorescence was examined by a fluorescent microscope (Zeiss). Fluorescence intensity was measured using Image J software. Results were presented as a ratio of the fluorescent area relative to each cross-section.

The MMP activity in the FBS-free conditioned media from cell cultures was quantified using gelatin zymography as we previously described (Liu et al., 2015).

2.16 Systolic blood pressure measurement

A tail-cuff device (BP-2000, Visitech Systems) was used to monitor the systolic blood pressure on day 0 before minipumps installation and on day 28 after Ang II treatment. Furthermore, each mouse's systolic blood pressure was measured three times, and the mean value was calculated.

2.17 Statistical analysis

The data were represented as the mean ± standard error of mean (SEM) from a minimum of three separate *in vitro* studies or six mice per group for *in vivo* studies. Statistical analyses were conducted using GraphPad Prism v8.00. Homogeneity of variance was assessed via the Brown-Forsythe test or F test. Two-group comparisons were performed with a two-tailed t-test with or without Welch's correction when normal distribution was satisfied. Otherwise, a nonparametric test was used for data sets with a non-normal distribution. One-way ANOVA with Bonferroni post-hoc analysis was used for more than two groups. Fisher's exact test was employed to determine the statistical significance of the differences in the incidence of aneurysms

among the groups. Mouse survival rates were examined by plotting Kaplan-Meier survival curves and assessing the differences using the log-rank (Mantel-Cox) test. The statistical significance was set at level of $P < 0.05$.

3. Results

3.1 Pterostilbene treatment effect on Ang II-induced AAA formation

To assess the impact of Pt on the initiation and progression of AAA, ApoE$^{-/-}$ mice received low or high doses of Pt the day after Ang II-induced AAA initiation (Fig. 1B). By day 28 post mini-pump implantation, the majority of mice in the Ang II group displayed obvious abdominal aortic aneurysms compared to the Saline group, whereas Pt treatment effectively prevented AAA formation in a dose-dependent manner (Fig. 1C). Five ApoE$^{-/-}$ mice died suffering from thoracic aortic dissection (n = 1) and AAA rupture (n = 4), and eight ApoE$^{-/-}$ mice developed suprarenal aneurysm in the Ang II group. In contrast, only three mice in the Pt-L + Ang II group and one mouse in the Pt-H + Ang II group died due to AAA rupture. Furthermore, four mice in the Pt-L + Ang II group and two mice in the Pt-H + Ang II group developed suprarenal abdominal aortic aneurysms. The incidence of aneurysm formation or rupture was lower in the Pt-L + Ang II group (46.7%, 7/15) and the Pt-H + Ang II group (20.0%, 3/15) than in the Ang II group (80.0%, 12/15, Fig. 1D, Fig. S1A). Consistently, Pt substantially decreased the maximal diameter of the abdominal aorta (Fig. 1E). In addition, systolic blood pressure after Ang II infusion did not show any variation after Pt treatment (Fig. S1B).

AAA is characterized by degradation of the extracellular matrix (ECM). The presence of collagen and elastin in the ECM is crucial for maintaining the elasticity and structural integrity of blood vessels. The aortic wall was evaluated for vascular remodeling using H&E, EVG, and Masson's trichrome staining. The mice in the Ang II group exhibited noticeable deviations in the aortic architecture with irregular arrangements, increased collagen fibers, and reduced elastic fibers compared to the

Saline group (Fig. 1F-H, Fig. S1C). However, dissecting aneurysms and elastin fragmentation were alleviated by Pt treatment (Fig. 1F-H, Fig. S1C).

MMPs, such as MMP2, MMP3, and MMP9, facilitate matrix degradation, which impairs the degradation of the arterial wall and favors aneurysm development (Carmeliet et al., 1997; Hadi et al., 2018). WB analysis and *in situ* MMP activity measurement revealed a substantial reduction in the levels of MMPs in the aortas from Pt-gavaged group compared with the Ang II group (Fig. 1I-J). Accordingly, a strong increase of MMP2 and MMP3 caused by Ang II was effectively inhibited by Pt treatment in the aortic media and adventitia of diseased aortas, notably in SMCs in the aorta media (Fig. 2A-B). Furthermore, Ang II-treated mice were accompanied by a marked decrease of the contractile-state phenotypic markers (α-SMA and CNN1) in SMCs, whereas mice treated with Pt showed reduced levels of α-SMA and CNN1 (Fig. 2C-D). Moreover, we evaluated the level of vascular cell adhesion molecule 1 (VCAM-1) and observed a reduction in its level of expression in the Pt-treated group (Fig. 2E). Furthermore, inflammatory cell infiltration as determined by CD68 staining was reduced in the Pt-treated group (Fig. 2F). Adding to the numerous therapeutic effects, Pt treatment was demonstrated to enhance eNOS phosphorylation in the vascular endothelial cells (Fig. S1D), indicating an improvement in endothelial function.

3.2 Pterostilbene regulated the inflammatory status and VSMC phenotypic switching in VSMCs

VSMC inflammation and contractile to synthetic state phenotypic switching contribute to AAA formation and development (Golledge, 2019). Therefore, we used primary RASMCs *in vitro* to investigate the effects of Pt on inflammatory status and phenotypic switching of VSMCs. CCK-8, used to assess cell viability, demonstrated that the activity of RASMCs was unaffected by the concentration of Pt 1-50 μM (Fig. 2G). Interestingly, similar to the broad-spectrum MMP inhibitor, doxycycline, Pt inhibited MMP activity to a similar extent, as evidenced by quantitative gelatin

zymography (Miow et al., 2021) (Fig. S2A). WB analysis showed reduced protein expression of MMPs and VCAM-1 in Pt and TNF-α-treated RASMCs, compared to treatment with TNF-α alone (Fig. 2H). Additionally, the inhibitory activity of Pt on MMPs was further validated in MASMCs (Fig. S2B). Consistently, Pt markedly decreased mRNA expression of MMPs induced by TNF-α in RASMCs in a dose-dependent manner (Fig. S2C). Moreover, Pt also countered TNF-α-induced deleterious changes in α-SMA, SM22α, and elastin expression (Fig. 2I). These data indicate that Pt is able to suppress VSMC inflammation and maintain VSMC homeostasis *in vitro*.

3.3 Pt exerted antioxidant and anti-inflammatory effects in VSMCs via activating the KEAP1/Nrf2 pathway

To explore the potential therapeutic targets of Pt on AAA, RNA sequencing was conducted to identify genes that are expressed differentially in RASMC mRNA profiles upon co-treatment with Pt plus TNF-α or TNF-α alone. The results showed that a collective of 246 genes exhibited an upregulation in response to Pt, with *Hmox-1* and *Nqo1* showing the most pronounced upregulation (Fig. 3A). Notably, KEGG analysis indicated that Pt induced upregulation of genes implicated in the KEAP1-Nrf2 pathway and downregulation of the cytosolic DNA-sensing pathway (Fig. 3B). GO analysis also revealed the involvement of genes in the pathways associated with Nrf2 and STING, such as oxidative stress, inflammation, and innate immune responses (Fig. 3C). A heatmap was generated to illustrate the significant activation of Nrf2 and its downstream targets by Pt in RASMCs, with further qPCR analysis confirming the upregulation of genes pivotal for combating oxidative stress and inflammation (Fig. 3D-E).

Correspondingly, we observed a significant elevation of Nrf2 and HO-1 levels in the aortic tissues of mice treated with Pt (Fig. 4A-B, Fig. S3A). In line with these observations, Pt treatment downregulated KEAP1 while enhancing Nrf2 expression in RASMCs, subsequently amplifying the RNA and protein expression of Nrf2

downstream targets, including HO-1, GCLM, and NQO1 (Fig. S3B-C). TBHQ, a widely used Nrf2 activator (Xu et al., 2022), was used as a positive control and similarly increased Nrf2 and the expression of its downstream targets, validating the effectiveness of Nrf2 activation in the study. Pt also effectively upregulated Nrf2 and its downstream target genes in MASMCs (Fig. S3D).

Under basal conditions, KEAP1 suppresses the activity of Nrf2. However, Nrf2 is released from the inhibitory effect of KEAP1 when it binds to other molecules in competition with KEAP1 (Itoh et al., 1999; Ren et al., 2021; Yamamoto et al., 2018). Immunofluorescence staining and WB analysis demonstrated that Pt freed Nrf2 and enhanced the expression and translocation of Nrf2 (Fig. 4C-D). These observations indicate that Pt competitively binds KEAP1 and functionally liberates Nrf2 transactivation activity from repression by Keap1. To obtain further insights on how Pt activates the KEAP1/Nrf2 signaling pathway, we performed a molecular docking analysis to infer whether or not there is a direct interaction between Pt and KEAP1/Nrf2. The molecular docking showed that Pt exhibits the highest affinity with the arginine triad residues (R415, R483) of KEAP1 kelch domain (Fig. 4E). As further confirmation of the binding, we showed in CETSA that Pt heat-stabilized KEAP1 (Fig. 4F). This interaction was further confirmed by an isothermal dose-response fingerprint CETSA (ITDRF-CETSA) study. Pt stabilized the KEAP1 protein and bound to it in a dose-dependent manner (from 0 to 102.4 μM, IC_{50} = 2.9 μM, Fig. 4G).

3.4 Pt inhibited mtDNA-STING-NF-κB pathway in VSMCs by activating Nrf2

An aberration in the generation and elimination of ROS, leading to the excessive creation of harmful oxidative substances, has been suggested to contribute to AAA (Miller et al., 2002). Typically, ROS levels are homeostatically maintained by a responsive antioxidant system that reacts to cellular stresses. The transcription factor Nrf2 primarily governs the regulation of this system (DeNicola et al., 2011). Therefore, we investigated whether Pt reduces ROS production. As shown in Fig. 5A,

Pt treatment reversed ROS production in the vessel wall of Ang II-treated ApoE$^{-/-}$mice. Consistently, the quantitative results of flow cytometry revealed that total concentrations of ROS in the Pt-treated RASMCs were lower than those in the cells treated with TNF-α alone (Fig. 5B).

Excessive ROS can lead to mitochondrial damage, including perturbed mitochondrial dynamics such as mitochondrial fusion and fission, which contribute to the pathogenesis underlying the formation and progression of AAA (Cooper et al., 2021). Mitofusin2 (MFN2)-mediated mitochondrial fusion suppresses ROS generation and prevents mitochondrial fragmentation (Ashraf and Kumar, 2022). Mitochondrial fission is predominately driven by dynamin-related protein 1 (DRP1), which is enhanced in human AAA samples in comparison with age-matched healthy controls (Cooper et al., 2021; Kleele et al., 2021). Voltage dependent anion channel 1 (VDAC1) is also an essential protein in mitochondria to maintain normal functions (Geisler et al., 2010). Overexpression of VDAC1 to form oligomers leads to cell apoptosis, inflammation, and the release of mtDNA (Xian et al., 2022). As shown in Fig. S4A, Pt increased the expression of MFN2 while inhibiting the expression of DRP1 and VDAC1 induced by TNF-α in RASMCs, suggesting that the mitochondrial damage was rescued by Pt.

Overproduction of ROS and mitochondrial damage cause the release of mtDNA, which in turn initiates a cycle of events that leads to further ROS production and activation of inflammatory factors (He et al., 2022). With the release of mtDNA into the cytosol, the DNA sensor cGAS recruits STING to associate with cytosolic-free DNA (cfDNA), which induces the production of cyclic GMP-AMP (cGAMP) (Shpilka and Haynes, 2018; Song et al., 2023). Activated STING recruits downstream kinases such as TBK1 (tank-binding kinase 1) to activate both IRF3 and NF-κB that mediate immune defense and inflammatory responses (Decout et al., 2021; Luo et al., 2020; Zhang et al., 2019). Thus, vascular inflammation and damage are facilitated by aberrant STING activity (Wu et al., 2022). Because Pt was able to induce Nrf2

activation, suppress ROS production, and reduce mitochondrial damage in VSMCs, we postulated that Pt could influence the activation of the STING pathway by controlling mtDNA release. Exposing RASMCs to TNF-α resulted in a rise in the buildup of tiny dsDNA particles outside mitochondria, while Pt-treatment decreased TNF-α-induced dsDNA quantity (Fig. 5C). The quantification of DNA in the cytosolic fraction revealed an augmentation in the quantity of cytosolic dsDNA in TNF-α-treated RASMCs, while Pt reversed this effect (Fig. 5D-E). We then examined the cytosolic DNA via qPCR analysis using primers that were specific for ribosome and mtDNA DNA sequences. mtDNA was the primary source of cytosolic dsDNA in TNF-α-treated RASMCs, while Pt was able to block the mtDNA release into the cytoplasm under TNF-α treatment conditions (Fig. 5F). Accordingly, the expression of STING was reduced in mice given Ang II infusions after Pt treatment (Fig. 5G-H). Furthermore, the activation of STING and downstream inflammatory pathways were all reversed by Pt treatment in RASMCs, as evidenced by decreased levels of p-STING, p-TBK1, p-IRF3, and p-NF-κB (Fig. S4B-C). H151, a potent and selective antagonist of STING (Haag et al., 2018), was applied as a positive control and inhibited the activation of STING and its downstream signaling. Similarly, Pt also attenuated the STING signaling pathway in MASMCs (Fig. S4D).

The generation of mitochondrial ROS is associated with mitochondrial damage as well as mtDNA release, a process that is regulated by the KEAP1/Nrf2 pathway, so we postulated that Pt suppressed the STING pathway via Nrf2 activation in VSMCs. To test this hypothesis, ML385, a selective inhibitor of Nrf2, was administered as a pre-treatment to RASMCs. Consistently, the quantitative results of flow cytometry revealed that ML385 abrogated that Pt inhibited total concentrations of ROS induced by TNF-α-induced activation in RASMCs (Fig. 6A). WB analysis showed that ML385 abrogated the suppressive impact of Pt on the STING pathway in RASMCs (Fig. 6B), suggesting that Pt inhibited the STING signaling pathway at least partially through activating Nrf2. Furthermore, ML385 inhibited the protective effects of Pt on VSMC inflammation and contractile-state phenotype, as evidenced by WB analysis or

qPCR analysis of MMPs, inflammatory cytokines, and contractile-state markers *in vitro* (Fig. 6C-E). These findings suggest that Pt promotes VSMC homeostasis by activating the Nrf2 pathway *in vitro*.

3.5 VSMC-specific Nrf2 deficiency diminished the protective effect of Pt against Ang II-induced AAA in mice

To investigate whether or not Pt suppressed STING activation and AAA formation through activating Nrf2 in VSMCs *in vivo*, we generated a VSMC-specific adeno-associated viral (AAV) serotype 2 vector containing a combination of VSMC-specific promoters (SM22α promoter) along with GFP protein and a mouse sh-Nrf2 sequence to knock down Nrf2 (AAV-sh-Nrf2, Fig. S5A). $ApoE^{-/-}$ mice were injected with AAV-sh-Nrf2 (to induce Nrf2 knockdown) or administered a control virus (AAV-sh-control) for two weeks. Fluorescence imaging of tissues showed that the AAV specifically infected the aorta and that GFP protein was specifically expressed in the aortic vessels (Fig. 7A). Cross-sections of the aorta in the AAV-sh-control group and the AAV-sh-Nrf2 group show GFP expression in the smooth muscle layer (Fig. S5B). After confirming the efficacy of AAV, we first administered the AAV to mice and then established a mouse AAA model generated by Ang II using the previously described protocol (Fig. 7B). The AAV-sh-Nrf2-treated mice showed a notably decreased Nrf2 protein expression in the medial VSMCs of the aorta, but not in the brain tissue, which has few SMCs, highlighting the SMC-specific knockdown. Consistently, the VSMC-specific Nrf2 knockdown abolished the ability of Pt to reduce the incidence of AAA and the maximal diameter of the abdominal aorta (Fig. 7E-H). Compared to the Pt + AAV-sh-control group, the mice in the Pt + AAV-sh-Nrf2 group exhibited anomalies in the aortic architecture with irregular structural arrangements, increased collagen fibers, and fewer elastic fibers (Fig. 7I-K). Moreover, immunostaining showed that Pt-mediated downregulation of MMP2, MMP3, VCAM-1, CD68, and STING and upregulation of a-SMA were largely abrogated by Nrf2 knockdown in VSMCs (Fig. 8A-B). Consistently, WB analysis

revealed that VSMC-specific Nrf2 knockdown abolished the capacity of Pt to reduce protein expression of MMP2, MMP9, p-STING, p-TBK1, and p-IRF3 induced by Ang II (Fig. 8C-D). Overall, these findings highlight the critical role of Nrf2 activation in VSMCs in Pt-mediated inhibitory effects on STING pathway and protective effects on AAA formation *in vivo*.

4. Discussion

This research presents evidence that Pt is an anti-aneurysm drug candidate that suppresses the formation of AAA in a validated and clinically relevant mouse model of the disease. Pt exerts a significant impact on reducing oxidative stress and inflammation via activating the KEAP1-Nrf2 pathway in VSMCs during the development of AAA. Importantly, our study identified Pt as a potent STING inhibitor to suppress vascular inflammation and maintain vascular homeostasis, thereby offering a novel perspective on the processes by which Pt inhibits AAA (Fig. 9).

AAA is a severe vascular disease with a high mortality rate associated with vessel rupture. Pharmacological intervention is needed to inhibit AAA expansion and prevent aneurysm rupture. Presenting results describing Pt as a promising medication in an animal model provides valuable insights into the pathology and future clinical therapy of patients with AAA. Pt is a naturally occurring polyphenol present in blueberries and several grape varieties, and its anti-inflammatory and antioxidant properties have been widely recognized (Estrela et al., 2013). Due to the high demand for Pt, researchers have developed an approach based on metabolic engineering to produce Pt naturally (Martínez-Márquez et al., 2016). Pt also has good bioavailability, and there are many Pt capsules and tablets commercially available (Lin et al., 2020). Moreover, research is underway to further improve the therapeutic efficacy of Pt via formulation optimization or structural modification. Recently, a nanoemulsion form of Pt was established, showing better release stability and optimized particle size to improve its bioavailability (Liu et al., 2024; Yang et al., 2023). Chen et al. engineered

alterations to the Pt molecular framework, culminating in the synthesis of the novel anti-inflammatory compound E2, which shows an enhanced safety profile and potent anti-inflammatory effects through strategic structural modifications of its chemical scaffold (Chen et al., 2024).

The prevention of vascular disorders by Pt may include pleiotropic effects. Firstly, as a PPARα agonism, Pt ameliorates dyslipidemia to protect blood vessels from atherosclerotic complications (Rimando et al., 2005). A recent study showed a significant reduction in levels of triglycerides (TG), total cholesterol (TC), very-low-density lipoprotein (VLDL), and low-density lipoprotein (LDL) with a concomitant increase in high-density lipoprotein (HDL) after Pt treatment, indicating that Pt decreases blood lipid accumulation in tyloxapol-induced mice (Shen et al., 2023). In line with this study, de Morais et al. also showed that Pt treatment improved lipid profiles, including reduced TG and VLDL levels in rats fed sucrose solution (de Morais et al., 2021). These findings suggest that Pt has a beneficial effect on the lipid profile, which might contribute to the Pt-mediated protective effect on AAA formation in $ApoE^{-/-}$ mice. Secondly, Pt inhibited neutrophil infiltration and the generation of pro-inflammatory mediators by activating the KEAP1/Nrf2 signaling and limiting the NF-κB and NLRP3 pathways (Yang et al., 2020), which is partially compatible with our results. Additionally, Pt down-regulated the level of MMPs and suppressed edema, cellular disintegration, macrophage infiltration, and polymorphonuclear leucocyte degranulation against cerebral ischemia/reperfusion injury in rats (Yan et al., 2021). These protective properties of Pt mentioned above might be at least partially responsible for its anti-aneurysm action demonstrated in the current studies. AAA has features distinct from these diseases thus, we can speculate that there are other mechanisms responsible for the effectiveness of Pt against AAA.

Previous studies have shown that Pt ameliorates oxidative damage in human keratinocytes (Zhou et al., 2019) and human ovarian granulosa cells (Chen et al., 2023) by activating the Nrf2 pathway. However, whether and how Pt regulates the Nrf2

pathway in VSMCs and participates in the pathogenesis of AAA remains unclear. In this research, we found that Pt suppressed the occurrence and mortality of AAA in Ang II-induced ApoE$^{-/-}$ mice. RNA-seq revealed that Pt activated Nrf2 and promoted the expression of Nrf2-dependent genes involved in antioxidant and anti-inflammatory processes in VSMCs, notably HO-1 and NQO1 (Zhang et al., 2022a). Molecular docking, CETSA, and ITDRF-CETSA methods demonstrated that Pt was competitively bound to KEAP1, and then Nrf2 translocated into the nucleus. Importantly, VSMC-specific knockdown of Nrf2 largely abrogated the protective role of Pt in AAA in vivo, indicating a crucial role of the KEAP1/Nrf2 pathway in the Pt-mediated effect on AAA. Emerging evidence suggests that STING is overexpressed in arterial aneurysm and that STING-mediated vascular inflammation remains critical in AAA pathogenesis. According to recent research, Nrf2 suppresses STING by lowering the stability of STING mRNA in mouse dopaminergic neurons and human epithelial cells (Olagnier et al., 2018; Zhao et al., 2021). However, it remains to be seen whether and how Pt-mediated KEAP1-Nrf2 activation regulates STING expression and STING downstream inflammatory activation pathways in VSMCs during AAA formation.

Under physiological conditions, Nrf2 is bound to KEAP1 in the cytoplasm. Under conditions of oxidative stress, the link between Nrf2 and KEAP1 breaks, allowing activated Nrf2 to enter the nucleus. Once inside the nucleus, Nrf2 interacts with ARE to activate downstream antioxidant enzymes, particularly HO-1, thereby limiting the generation of ROS (Sies et al., 2017). ROS is directly linked to matrix destruction and aneurysm formation (Sánchez-Infantes et al., 2021). ROS accumulation also induces mtDNA to escape from stressed mitochondria (Shokolenko et al., 2009). dsDNA is crucial for aortic degeneration and AAA formation due to its role in promoting SMC damage, MMP synthesis, and ECM degeneration (Luo et al., 2020). Notably, RNA-seq revealed the involvement of genes in the pathways associated with both Nrf2 and the cytosolic DNA-sensing pathways (Fig. 3B). Intriguingly, our studies support the hypothesis that Pt reduced ROS and oxidative

stress, mitigated mitochondrial damage, thus reducing the release of mtDNA, and subsequently inhibited the cGAS-STING-TBK1-NF-κB signaling pathway to reduce VSMC inflammation. Taken together, our findings indicate that Pt inhibits STING-mediated vascular inflammation and preserves vascular homeostasis by activating the Nrf2 pathway in AAA.

Vascular inflammation initiates the aortic wall's degradation via inflammatory cell recruitment and proteolytic enzyme secretion, thereby driving AAA formation and progression (Huang et al., 2023). Concurrently, VSMC phenotypic shift to a synthetic state, characterized by heightened extracellular matrix output and increased migration, exacerbates the aortic wall's pathological alteration. These mechanisms are crucial in AAA development and progression (Lai et al., 2020). Our study is in concordance with these findings, indicating that Pt exerts anti-AAA activity through multiple molecular mechanisms, including promoting VSMC homeostasis and an anti-inflammatory phenotype within the AAA disease state.

Previously, Kaneko et al. reported that resveratrol, another naturally occurring polyphenolic compound that has a similar chemical structure to Pt, prevents the formation of $CaCl_2$-induced AAA by reducing inflammation, oxidative stress, extracellular matrix (ECM) degradation and the activity of MMPs (Kaneko et al., 2011), which is similar to the results with Pt obtained in our study. Of note, Pt exhibits higher bioavailability and metabolic stability compared to resveratrol due to the presence of two methoxy groups (-OCH3) at the C-3 and C-5 positions, which facilitate Pt's capacity to permeate cell membranes and slow down cell metabolism in the body. In terms of pharmacological activity, Pt exhibits stronger activities in lipid-lowering, cellular stress response, and anti-inflammatory effects compared to resveratrol (Chang et al., 2012; Gómez-Zorita et al., 2014). Furthermore, Pt is more effective in mediating antitumor actions by activating the Nrf2 signaling pathway and inducing its target genes, such as HO-1 (Chiou et al., 2011). These properties may

position Pt as a more promising candidate in future drug development and therapeutic strategies.

Most recently, Cai et al. specified a different mechanism by which Pt can inhibit macrophage pyroptosis through the miR-146a-5p/TRAF6 axis to mitigate AAA (Cai et al., 2024). Those two independent pieces of work arrive at essentially the same conclusions about Pt in AAA formation, which added weight to the results of both studies. Besides, our study contributes to existing knowledge and advances the field by revealing that Pt mitigates AAA by targeting the KEAP1-Nrf2-mtDNA-STING-TBK1 axis in VSMCs, thereby offering a novel perspective on the processes by which Pt inhibits AAA. Accumulating evidence indicates that the abnormal activation of the STING pathway in endothelial cells and macrophages also contributes to the development of CVDs (Luo et al., 2020; Oduro et al., 2022; Xuesong Li, 2023). Moreover, our study showed that Pt activates eNOS in endothelial cells, suggesting an improvement in endothelial function. Therefore, whether Pt also exerts anti-aneurysm effects through actions on other cell types, such as macrophages and endothelial cells, warrants further investigation.

The current study provides substantial evidence *in vivo* and *in vitro* that the therapeutic effects of Pt against AAA are primarily dependent on activation of Nrf2 signaling in VSMCs. Importantly, activation of Nrf2 was shown to be a key mechanism by which Pt inhibits the STING pathway. This work elucidates the mechanistic understanding of Pt in the amelioration of AAA and sets the stage for future consideration of the KEAP1-Nrf2-STING axis as an innovative strategy for the development of therapeutic agents to address the severe human disease of AAA.

Author contributions

Zhiping Liu designed the study. Jiami Zou, Zhihua Zheng, Weile Ye, Mei Jin, Pinglian Yang, and Jiaojiao Wang conducted experiments, acquired, analyzed and

interpreted the data. Jiami Zou drafted the manuscript. Jiaojiao Wang, Peter J Little and Zhiping Liu critically reviewed and revised the manuscript and provided insights in the area of vascular smooth muscle cell biology. All authors have read and approved the submitted manuscript. All data were generated in-house, and no paper mill was used. All authors agree to be accountable for all aspects of work ensuring integrity and accuracy.

Declaration of competing interest

There are no competing interests declared by the authors.

Acknowledgements

This work is supported by National Natural Science Foundation of China (No. 82270500, 82203304) and Guangdong Basic and Applied Basic Research Foundation (No. 2024B1515020113).

References

Ashraf, R., Kumar, S., 2022. Mfn2-mediated mitochondrial fusion promotes autophagy and suppresses ovarian cancer progression by reducing ROS through AMPK/mTOR/ERK signaling. Cell Mol Life Sci 79, 573.

Behl, T., Bungau, S., Kumar, K., Zengin, G., Khan, F., Kumar, A., Kaur, R., Venkatachalam, T., Tit, D.M., Vesa, C.M., Barsan, G., Mosteanu, D.-E., 2020. Pleotropic Effects of Polyphenols in Cardiovascular System. Biomed Pharmacother 130, 110714.

Bossone, E., Eagle, K.A., 2021. Epidemiology and management of aortic disease: aortic aneurysms and acute aortic syndromes. Nat Rev Cardiol 18, 331-348.

Buck, D.B., van Herwaarden, J.A., Schermerhorn, M.L., Moll, F.L., 2014. Endovascular treatment of abdominal aortic aneurysms. Nat Rev Cardiol 11, 112-123.

Cai, H., Huang, L., Wang, M., Liu, R., Qiu, J., Qin, Y., Yao, X., Wang, S., Yao, C., Hu, Z., Zhou, Y., 2024. Pterostilbene alleviates abdominal aortic aneurysm via inhibiting macrophage pyroptosis by activating the miR-146a-5p/TRAF6 axis. Food Funct 15, 139-157.

Carmeliet, P., Moons, L., Lijnen, R., Baes, M., Lemaître, V., Tipping, P., Drew, A., Eeckhout, Y., Shapiro, S., Lupu, F., Collen, D., 1997. Urokinase-generated plasmin activates matrix metalloproteinases during aneurysm formation. Nat Genet 17, 439-444.

Chang, J., Rimando, A., Pallas, M., Camins, A., Porquet, D., Reeves, J., Shukitt-Hale, B., Smith, M.A., Joseph, J.A., Casadesus, G., 2012. Low-dose pterostilbene, but not resveratrol, is a potent neuromodulator in aging and Alzheimer's disease. Neurobiol Aging 33, 2062-2071.

Chen, L., Wang, K., Liu, X., Wang, L., Zou, H., Hu, S., Zhou, L., Li, R., Cao, S., Ruan, B., Cui, Q., 2024. Design, synthesis, in vitro and in vivo biological evaluation of pterostilbene derivatives for anti-inflammation therapy. J Enzyme Inhib Med Chem 39, 2315227.

Chen, X., Song, Q.L., Li, Z.H., Ji, R., Wang, J.Y., Cao, M.L., Mu, X.F., Zhang, Y., Guo, D.Y., Yang, J., 2023. Pterostilbene ameliorates oxidative damage and ferroptosis in human ovarian granulosa cells by regulating the Nrf2/HO-1 pathway. Arch Biochem Biophys 738, 109561.

Chiou, Y.-S., Tsai, M.-L., Nagabhushanam, K., Wang, Y.-J., Wu, C.-H., Ho, C.-T., Pan, M.-H., 2011. Pterostilbene is more potent than resveratrol in preventing azoxymethane (AOM)-induced colon tumorigenesis via activation of the NF-E2-related factor 2 (Nrf2)-mediated antioxidant

signaling pathway. J Agric Food Chem 59, 2725-2733.

Cooper, H.A., Cicalese, S., Preston, K.J., Kawai, T., Okuno, K., Choi, E.T., Kasahara, S., Uchida, H.A., Otaka, N., Scalia, R., Rizzo, V., Eguchi, S., 2021. Targeting mitochondrial fission as a potential therapeutic for abdominal aortic aneurysm. Cardiovasc Res 117, 971-982.

de Morais, J.M.B., Cruz, E.M.S., da Rosa, C.V.D., Cesário, R.C., Comar, J.F., Moreira, C.C.L., de Almeida Chuffa, L.G., Seiva, F.R.F., 2021. Pterostilbene influences glycemia and lipidemia and enhances antioxidant status in the liver of rats that consumed sucrose solution. Life Sci 269, 119048.

Decout, A., Katz, J.D., Venkatraman, S., Ablasser, A., 2021. The cGAS-STING pathway as a therapeutic target in inflammatory diseases. Nat Rev Immunol 21, 548-569.

DeNicola, G.M., Karreth, F.A., Humpton, T.J., Gopinathan, A., Wei, C., Frese, K., Mangal, D., Yu, K.H., Yeo, C.J., Calhoun, E.S., Scrimieri, F., Winter, J.M., Hruban, R.H., Iacobuzio-Donahue, C., Kern, S.E., Blair, I.A., Tuveson, D.A., 2011. Oncogene-induced Nrf2 transcription promotes ROS detoxification and tumorigenesis. Nature 475, 106-109.

Estrela, J.M., Ortega, A., Mena, S., Rodriguez, M.L., Asensi, M., 2013. Pterostilbene: Biomedical applications. Crit Rev Clin Lab Sci 50, 65-78.

Galyfos, G., Sigala, F., Mpananis, K., Vouros, D., Kimpizi, D., Theodoropoulos, C., Zografos, G., Filis, K., 2020. Small abdominal aortic aneurysms: Has anything changed so far? Trends Cardiovasc Med 30, 500-504.

Geisler, S., Holmström, K.M., Skujat, D., Fiesel, F.C., Rothfuss, O.C., Kahle, P.J., Springer, W., 2010. PINK1/Parkin-mediated mitophagy is dependent on VDAC1 and p62/SQSTM1. Nat Cell Biol 12, 119-131.

Golledge, J., 2019. Abdominal aortic aneurysm: update on pathogenesis and medical treatments. Nat Rev Cardiol 16, 225-242.

Gómez-Zorita, S., Fernández-Quintela, A., Lasa, A., Aguirre, L., Rimando, A.M., Portillo, M.P., 2014. Pterostilbene, a dimethyl ether derivative of resveratrol, reduces fat accumulation in rats fed an obesogenic diet. J Agric Food Chem 62, 8371-8378.

Haag, S.M., Gulen, M.F., Reymond, L., Gibelin, A., Abrami, L., Decout, A., Heymann, M., van der Goot, F.G., Turcatti, G., Behrendt, R., Ablasser, A., 2018. Targeting STING with covalent

small-molecule inhibitors. Nature 559, 269-273.

Hadi, T., Boytard, L., Silvestro, M., Alebrahim, D., Jacob, S., Feinstein, J., Barone, K., Spiro, W., Hutchison, S., Simon, R., Rateri, D., Pinet, F., Fenyo, D., Adelman, M., Moore, K.J., Eltzschig, H.K., Daugherty, A., Ramkhelawon, B., 2018. Macrophage-derived netrin-1 promotes abdominal aortic aneurysm formation by activating MMP3 in vascular smooth muscle cells. Nat Commun 9, 5022.

Hayden, M.S., Ghosh, S., 2008. Shared principles in NF-kappaB signaling. Cell 132, 344-362.

He, B., Yu, H., Liu, S., Wan, H., Fu, S., Liu, S., Yang, J., Zhang, Z., Huang, H., Li, Q., Wang, F., Jiang, Z., Liu, Q., Jiang, H., 2022. Mitochondrial cristae architecture protects against mtDNA release and inflammation. Cell Rep 41, 111774.

Ho, Y.C., Wu, M.L., Gung, P.Y., Chen, C.H., Kuo, C.C., Yet, S.F., 2016. Heme oxygenase-1 deficiency exacerbates angiotensin II-induced aortic aneurysm in mice. Oncotarget 7, 67760-67776.

Huang, S.-E., Kuo, C.-H., Shiao, S.-Y., Shen, C.-R., Lee, F.-T., Chang, B.-I., Hsu, J.-H., Wu, H.-L., Yeh, J.-L., Lai, C.-H., 2023. Soluble CD93 lectin-like domain sequesters HMGB1 to ameliorate inflammatory diseases. Theranostics 13, 4059-4078.

Itoh, K., Wakabayashi, N., Katoh, Y., Ishii, T., Igarashi, K., Engel, J.D., Yamamoto, M., 1999. Keap1 represses nuclear activation of antioxidant responsive elements by Nrf2 through binding to the amino-terminal Neh2 domain. Genes Dev 13, 76-86.

Kaneko, H., Anzai, T., Morisawa, M., Kohno, T., Nagai, T., Anzai, A., Takahashi, T., Shimoda, M., Sasaki, A., Maekawa, Y., Yoshimura, K., Aoki, H., Tsubota, K., Yoshikawa, T., Okada, Y., Ogawa, S., Fukuda, K., 2011. Resveratrol prevents the development of abdominal aortic aneurysm through attenuation of inflammation, oxidative stress, and neovascularization. Atherosclerosis 217, 350-357.

Kim, H.-S., Quon, M.J., Kim, J.-A., 2014. New insights into the mechanisms of polyphenols beyond antioxidant properties; lessons from the green tea polyphenol, epigallocatechin 3-gallate. Redox Biol 2, 187-195.

Kleele, T., Rey, T., Winter, J., Zaganelli, S., Mahecic, D., Perreten Lambert, H., Ruberto, F.P., Nemir, M., Wai, T., Pedrazzini, T., Manley, S., 2021. Distinct fission signatures predict

mitochondrial degradation or biogenesis. Nature 593, 435-439.

Kobayashi, E.H., Suzuki, T., Funayama, R., Nagashima, T., Hayashi, M., Sekine, H., Tanaka, N., Moriguchi, T., Motohashi, H., Nakayama, K., Yamamoto, M., 2016. Nrf2 suppresses macrophage inflammatory response by blocking proinflammatory cytokine transcription. Nat Commun 7, 11624.

Lai, C.-H., Chang, C.-W., Lee, F.-T., Kuo, C.-H., Hsu, J.-H., Liu, C.-P., Wu, H.-L., Yeh, J.-L., 2020. Targeting vascular smooth muscle cell dysfunction with xanthine derivative KMUP-3 inhibits abdominal aortic aneurysm in mice. Atherosclerosis 297, 16-24.

Li, X., Chen, X., Zheng, L., Chen, M., Zhang, Y., Zhu, R., Chen, J., Gu, J., Yin, Q., Jiang, H., Wu, X., Ji, X., Tang, X., Dong, M., Li, Q., Gao, Y., Chen, H., 2023. Non-canonical STING-PERK pathway dependent epigenetic regulation of vascular endothelial dysfunction via integrating IRF3 and NF-κB in inflammatory response. Acta Pharmaceutica Sinica. B 13, 4765-4784.

Lin, W.-S., Leland, J.V., Ho, C.-T., Pan, M.-H., 2020. Occurrence, Bioavailability, Anti-inflammatory, and Anticancer Effects of Pterostilbene. J Agric Food Chem 68, 12788-12799.

Liu, H., Zhao, L., Yue, L., Wang, B., Li, X., Guo, H., Ma, Y., Yao, C., Gao, L., Deng, J., Li, L., Feng, D., Qu, Y., 2017. Pterostilbene Attenuates Early Brain Injury Following Subarachnoid Hemorrhage via Inhibition of the NLRP3 Inflammasome and Nox2-Related Oxidative Stress. Mol Neurobiol 54, 5928-5940.

Liu, J., Xu, J., Jia, L., Zhou, Y., Fu, Q., Wang, Y., Mu, D., Wang, D., Li, N., Hou, Y., 2024. Pterostilbene nanoemulsion promotes Nrf2 signaling pathway to downregulate oxidative stress for treating Alzheimer's disease. Int J Pharm 655, 124002.

Liu, Z.P., Xu, S.W., Huang, X.Y., Wang, J.J., Gao, S., Li, H., Zhou, C.H., Ye, J.T., Chen, S.R., Jin, Z.G., Liu, P.Q., 2015. Cryptotanshinone, an orally bioactive herbal compound from Danshen, attenuates atherosclerosis in apolipoprotein E-deficient mice: role of lectin-like oxidized LDL receptor-1 (LOX-1). Brit J Pharmacol 172, 5661-5675.

Lu, H., Sun, J., Liang, W., Chang, Z., Rom, O., Zhao, Y., Zhao, G., Xiong, W., Wang, H., Zhu, T., Guo, Y., Chang, L., Garcia-Barrio, M.T., Zhang, J., Chen, Y.E., Fan, Y., 2020. Cyclodextrin Prevents Abdominal Aortic Aneurysm via Activation of Vascular Smooth Muscle Cell Transcription Factor EB. Circulation 142, 483-498.

Luo, W., Wang, Y., Zhang, L., Ren, P., Zhang, C., Li, Y., Azares, A.R., Zhang, M., Guo, J., Ghaghada, K.B., Starosolski, Z.A., Rajapakshe, K., Coarfa, C., Li, Y., Chen, R., Fujiwara, K., Abe, J.-I., Coselli, J.S., Milewicz, D.M., LeMaire, S.A., Shen, Y.H., 2020. Critical Role of Cytosolic DNA and Its Sensing Adaptor STING in Aortic Degeneration, Dissection, and Rupture. Circulation 141, 42-66.

Ma, Q., Yang, Q., Xu, J., Zhang, X., Kim, D., Liu, Z., Da, Q., Mao, X., Zhou, Y., Cai, Y., Pareek, V., Kim, H.W., Wu, G., Dong, Z., Song, W.-L., Gan, L., Zhang, C., Hong, M., Benkovic, S.J., Weintraub, N.L., Fulton, D., Asara, J.M., Ben-Sahra, I., Huo, Y., 2022. ATIC-Associated De Novo Purine Synthesis Is Critically Involved in Proliferative Arterial Disease. Circulation 146, 1444-1460.

Martínez-Márquez, A., Morante-Carriel, J.A., Ramírez-Estrada, K., Cusidó, R.M., Palazon, J., Bru-Martínez, R., 2016. Production of highly bioactive resveratrol analogues pterostilbene and piceatannol in metabolically engineered grapevine cell cultures. Plant Biotechnol J 14, 1813-1825.

Miller, F.J., Sharp, W.J., Fang, X., Oberley, L.W., Oberley, T.D., Weintraub, N.L., 2002. Oxidative stress in human abdominal aortic aneurysms: a potential mediator of aneurysmal remodeling. Arterioscler Thromb Vasc Biol 22, 560-565.

Miow, Q.H., Vallejo, A.F., Wang, Y., Hong, J.M., Bai, C., Teo, F.S., Wang, A.D., Loh, H.R., Tan, T.Z., Ding, Y., She, H.W., Gan, S.H., Paton, N.I., Lum, J., Tay, A., Chee, C.B., Tambyah, P.A., Polak, M.E., Wang, Y.T., Singhal, A., Elkington, P.T., Friedland, J.S., Ong, C.W., 2021. Doxycycline host-directed therapy in human pulmonary tuberculosis. J Clin Invest 131.

Mohamed, E., Sierra, R.A., Trillo-Tinoco, J., Cao, Y., Innamarato, P., Payne, K.K., de Mingo Pulido, A., Mandula, J., Zhang, S., Thevenot, P., Biswas, S., Abdalla, S.K., Costich, T.L., Hänggi, K., Anadon, C.M., Flores, E.R., Haura, E.B., Mehrotra, S., Pilon-Thomas, S., Ruffell, B., Munn, D.H., Cubillos-Ruiz, J.R., Conejo-Garcia, J.R., Rodriguez, P.C., 2020. The Unfolded Protein Response Mediator PERK Governs Myeloid Cell-Driven Immunosuppression in Tumors through Inhibition of STING Signaling. Immunity 52.

Oduro, P.K., Zheng, X., Wei, J., Yang, Y., Wang, Y., Zhang, H., Liu, E., Gao, X., Du, M., Wang, Q., 2022. The cGAS-STING signaling in cardiovascular and metabolic diseases: Future novel target option for pharmacotherapy. Acta Pharm Sin B 12, 50-75.

Olagnier, D., Brandtoft, A.M., Gunderstofte, C., Villadsen, N.L., Krapp, C., Thielke, A.L., Laustsen, A., Peri, S., Hansen, A.L., Bonefeld, L., Thyrsted, J., Bruun, V., Iversen, M.B., Lin, L., Artegoitia, V.M., Su, C., Yang, L., Lin, R., Balachandran, S., Luo, Y., Nyegaard, M., Marrero, B., Goldbach-Mansky, R., Motwani, M., Ryan, D.G., Fitzgerald, K.A., O'Neill, L.A., Hollensen, A.K., Damgaard, C.K., de Paoli, F.V., Bertram, H.C., Jakobsen, M.R., Poulsen, T.B., Holm, C.K., 2018. Nrf2 negatively regulates STING indicating a link between antiviral sensing and metabolic reprogramming. Nat Commun 9, 3506.

Park, E.-S., Lim, Y., Hong, J.-T., Yoo, H.-S., Lee, C.-K., Pyo, M.-Y., Yun, Y.-P., 2010. Pterostilbene, a natural dimethylated analog of resveratrol, inhibits rat aortic vascular smooth muscle cell proliferation by blocking Akt-dependent pathway. Vascul Pharmacol 53, 61-67.

Ren, X., Li, Y., Zhou, Y., Hu, W., Yang, C., Jing, Q., Zhou, C., Wang, X., Hu, J., Wang, L., Yang, J., Wang, H., Xu, H., Li, H., Tong, X., Wang, Y., Du, J., 2021. Overcoming the compensatory elevation of NRF2 renders hepatocellular carcinoma cells more vulnerable to disulfiram/copper-induced ferroptosis. Redox Biol 46, 102122.

Rimando, A.M., Nagmani, R., Feller, D.R., Yokoyama, W., 2005. Pterostilbene, a new agonist for the peroxisome proliferator-activated receptor alpha-isoform, lowers plasma lipoproteins and cholesterol in hypercholesterolemic hamsters. J Agric Food Chem 53, 3403-3407.

Sakalihasan, N., Limet, R., Defawe, O.D., 2005. Abdominal aortic aneurysm. Lancet 365, 1577-1589.

Sánchez-Infantes, D., Nus, M., Navas-Madroñal, M., Fité, J., Pérez, B., Barros-Membrilla, A.J., Soto, B., Martínez-González, J., Camacho, M., Rodriguez, C., Mallat, Z., Galán, M., 2021. Oxidative Stress and Inflammatory Markers in Abdominal Aortic Aneurysm. Antioxidants (Basel) 10.

Shen, B., Wang, Y., Cheng, J., Peng, Y., Zhang, Q., Li, Z., Zhao, L., Deng, X., Feng, H., 2023. Pterostilbene alleviated NAFLD via AMPK/mTOR signaling pathways and autophagy by promoting Nrf2. Phytomedicine : International Journal of Phytotherapy and Phytopharmacology 109, 154561.

Shokolenko, I., Venediktova, N., Bochkareva, A., Wilson, G.L., Alexeyev, M.F., 2009. Oxidative stress induces degradation of mitochondrial DNA. Nucleic Acids Res 37, 2539-2548.

Shpilka, T., Haynes, C.M., 2018. The mitochondrial UPR: mechanisms, physiological functions and implications in ageing. Nat Rev Mol Cell Biol 19, 109-120.

Sies, H., Berndt, C., Jones, D.P., 2017. Oxidative Stress. Annu Rev Biochem 86, 715-748.

Song, H., Xu, T., Feng, X., Lai, Y., Yang, Y., Zheng, H., He, X., Wei, G., Liao, W., Liao, Y., Zhong, L., Bin, J., 2020. Itaconate prevents abdominal aortic aneurysm formation through inhibiting inflammation via activation of Nrf2. EBioMedicine 57, 102832.

Song, J., Yang, R.-R., Chang, J., Liu, Y.-D., Lu, C.-H., Chen, L.-F., Guo, H., Zhang, Y.-H., Fan, Z.-S., Zhou, J.-Y., Zhou, G.-Z., Zhang, K.-K., Luo, X.-M., Chen, K.-X., Jiang, H.-L., Zhang, S.-L., Zheng, M.-Y., 2023. Discovery and characterization of a novel cGAS covalent inhibitor for the treatment of inflammatory bowel disease. Acta Pharmacol Sin 44, 791-800.

Thimmulappa, R.K., Lee, H., Rangasamy, T., Reddy, S.P., Yamamoto, M., Kensler, T.W., Biswal, S., 2006. Nrf2 is a critical regulator of the innate immune response and survival during experimental sepsis. J Clin Invest 116, 984-995.

Wu, B., Xu, M.-M., Fan, C., Feng, C.-L., Lu, Q.-K., Lu, H.-M., Xiang, C.-G., Bai, F., Wang, H.-Y., Wu, Y.-W., Tang, W., 2022. STING inhibitor ameliorates LPS-induced ALI by preventing vascular endothelial cells-mediated immune cells chemotaxis and adhesion. Acta Pharmacol Sin 43, 2055-2066.

Xian, H., Watari, K., Sanchez-Lopez, E., Offenberger, J., Onyuru, J., Sampath, H., Ying, W., Hoffman, H.M., Shadel, G.S., Karin, M., 2022. Oxidized DNA fragments exit mitochondria via mPTP- and VDAC-dependent channels to activate NLRP3 inflammasome and interferon signaling. Immunity 55.

Xu, J.K., Liu, J.Y., Li, Q., Li, G.X., Zhang, G.J., Mi, Y., Zhao, T., Mu, D.Y., Wang, D.Q., Zeng, K.W., Hou, Y., 2023. Pterostilbene participates in TLR4-mediated inflammatory response and autophagy-dependent Aβ1-42 endocytosis in Alzheimer's disease. Phytomedicine 119.

Xu, Y., Li, Y., Li, J., Chen, W., 2022. Ethyl carbamate triggers ferroptosis in liver through inhibiting GSH synthesis and suppressing Nrf2 activation. Redox Biol 53, 102349.

Xuesong Li, X.C., Longbin Zheng, Minghong Chen, Yunjia Zhang, Ruigong Zhu, et al., 2023. Non-canonical STING–PERK pathway dependent epigenetic regulation of vascular endothelial dysfunction via integrating IRF3 and NF-κB in inflammatory response. Acta Pharm Sin B 13,

4765-4784.

Yamamoto, M., Kensler, T.W., Motohashi, H., 2018. The KEAP1-NRF2 System: a Thiol-Based Sensor-Effector Apparatus for Maintaining Redox Homeostasis. Physiol Rev 98, 1169-1203.

Yan, W., Ren, D., Feng, X., Huang, J., Wang, D., Li, T., Zhang, D., 2021. Neuroprotective and Anti-Inflammatory Effect of Pterostilbene Against Cerebral Ischemia/Reperfusion Injury via Suppression of COX-2. Front Pharmacol 12, 770329.

Yang, H., Hua, C., Yang, X., Fan, X., Song, H., Peng, L., Ci, X., 2020. Pterostilbene prevents LPS-induced early pulmonary fibrosis by suppressing oxidative stress, inflammation and apoptosis in vivo. Food Funct 11, 4471-4484.

Yang, X., Liu, Z., Fang, M., Zou, T., Zhang, Z., Meng, X., Wang, T., Meng, H., Chen, Y., Duan, Y., Li, Q., 2023. Novel pterostilbene derivatives ameliorate heart failure by reducing oxidative stress and inflammation through regulating Nrf2/NF-κB signaling pathway. Eur J Med Chem 258, 115602.

Zettervall, S.L., Soden, P.A., Buck, D.B., Cronenwett, J.L., Goodney, P.P., Eslami, M.H., Lee, J.T., Schermerhorn, M.L., 2017. Significant regional variation exists in morbidity and mortality after repair of abdominal aortic aneurysm. J Vasc Surg 65, 1305-1312.

Zhang, C., Shang, G., Gui, X., Zhang, X., Bai, X.-C., Chen, Z.J., 2019. Structural basis of STING binding with and phosphorylation by TBK1. Nature 567, 394-398.

Zhang, Q., Wang, L., Wang, S., Cheng, H., Xu, L., Pei, G., Wang, Y., Fu, C., Jiang, Y., He, C., Wei, Q., 2022a. Signaling pathways and targeted therapy for myocardial infarction. Signal Transduct Target Ther 7, 78.

Zhang, Y., Murugesan, P., Huang, K., Cai, H., 2020. NADPH oxidases and oxidase crosstalk in cardiovascular diseases: novel therapeutic targets. Nat Rev Cardiol 17, 170-194.

Zhang, Y., Qiao, X., Liu, L., Han, W., Liu, Q., Wang, Y., Xie, T., Tang, Y., Wang, T., Meng, J., Ye, A., He, S., Chen, R., Chen, C., 2022b. Long noncoding RNA MAGI2-AS3 regulates the H2O2 level and cell senescence via HSPA8. Redox Biol 54, 102383.

Zhang, Y., Zhang, Y., 2016. Pterostilbene, a novel natural plant conduct, inhibits high fat-induced atherosclerosis inflammation via NF-κB signaling pathway in Toll-like receptor 5 (TLR5) deficient mice. Biomed Pharmacother 81, 345-355.

Zhao, M., Wang, B., Zhang, C., Su, Z., Guo, B., Zhao, Y., Zheng, R., 2021. The DJ1-Nrf2-STING axis mediates the neuroprotective effects of Withaferin A in Parkinson's disease. Cell Death Differ 28, 2517-2535.

Zhou, J., Ci, X., Ma, X., Yu, Q., Cui, Y., Zhen, Y., Li, S., 2019. Pterostilbene Activates the Nrf2-Dependent Antioxidant Response to Ameliorate Arsenic-Induced Intracellular Damage and Apoptosis in Human Keratinocytes. Front Pharmacol 10, 497.

Figure legends

Fig. 1. Pt regressed Ang II-induced AAA formation. (A) Chemical structure of Pt. (B) Schematic illustration of the animal experiment (n = 15 for each group). (C) Representative photographs of macroscopic appearance of aortas in the $ApoE^{-/-}$ mice. (D) AAA incidence. (E) Quantification analysis of the maximal suprarenal aorta diameter using a digital vernier caliper. (F-H) Representative images for H&E, EVG, and Masson trichrome staining of the mouse aortas, as well as elastin degradation scores. (I) Representative WB results of MMP2, MMP3, and MMP9 in mouse aorta samples. (J) *In situ* MMP activity assessment of aortic sections. Data are presented as mean ± SEM. $^{\#}P < 0.05$ and $^{\#\#\#}P < 0.001$ *vs.* Saline group; $^{*}P < 0.05$, $^{**}P < 0.01$, and $^{***}P < 0.001$ *vs.* Ang II group. Fisher's exact test for D, Brown-Forsythe ANOVA and Welch's ANOVA test with Dunnett's T3 multiple comparison for E, and one-way ANOVA followed by a Bonferroni post hoc analysis for I and J.

Fig. 2. Pt restrained inflammatory responses and VSMC phenotypic transition in AAA and TNF-α-induced VSMCs. (A-F) Representative immunohistochemical staining of serial sections showing the expression of MMP2, MMP3, α-SMA, CNN1, VCAM-1, and CD68 in indicated groups. (G) Cell viability was assessed by a CCK-8 assay. (H) WB analysis and quantification of the protein levels of MMP2, MMP3, MMP9, and VCAM-1 in RASMCs. (I) Protein expression (α-SMA, SM22α, and Elastin) measured by WB analysis in RASMCs. Data are presented as mean ± SEM. $^{\#\#\#}P < 0.001$ *vs.* Saline group in A-F; $^{**}P < 0.01$, and $^{***}P < 0.001$ *vs.* Ang II group in A-F; $^{\#\#}P < 0.01$, and $^{\#\#\#}P < 0.001$ *vs.* CT group in H-I; $^{*}P < 0.05$, $^{**}P < 0.01$, and $^{***}P < 0.001$ *vs.* TNF-α group in H-I; and ns means no significance. One-way ANOVA followed by a Bonferroni post hoc analysis for A-F and H-I, and an unpaired t-test for G.

Fig. 3. RNA sequencing revealed the upregulation of Nrf2 and its downstream target gene expression in Pt-treated RASMCs. RASMCs were pre-treated with Pt (10 μM) for 2 hours, followed by a 6-hour treatment with TNF-α (10 ng/mL). (A) The volcano plot illustrates the magnitude and significance of gene expression changes in TNF-α-stimulated versus Pt and TNF-α-co-treated RASMCs. Genes that were downregulated (left) and upregulated (right) by Pt treatment were shown as blue and red dots, respectively. (B) KEGG pathway analysis of

differentially expressed genes. (C) GO enrichment analysis of overlapped altered genes showing the 10 regulated terms. (D) Heatmap of genes upregulated by Pt are related to Nrf2 signaling pathway in the RNA-seq analysis. (E) qPCR assays confirmed the upregulation of *Hmox1*, *Nqo1*, *Txnrd1*, *Gclm*, *Gclc*, and *Fth1* in Pt-treated RASMCs, with *Gapdh* serving as the housekeeping gene for normalization. Data are presented as mean ± SEM. **P* < 0.05, ***P* < 0.01, and ****P* < 0.001 *vs.* TNF-α group; and ns means no significance. One-way ANOVA followed by a Bonferroni post hoc analysis for E.

Fig. 4. Nrf2 and its downstream target genes were activated in Pt-treated AAA tissues and VSMCs. (A) Representative immunostaining of Nrf2 and HO-1 in the suprarenal aortic wall sections. (B) WB analysis and quantification of the protein levels of Nrf2 and HO-1 protein levels in the aortas of ApoE$^{-/-}$ mice. (C) Nuclear-cytoplasmic separation followed by WB analysis of RASMCs in the indicated groups. (D) The distribution and localization of Nrf2 (green) in RASMCs were presented by immunofluorescence staining. (E) Molecular docking was used to detect the interaction between Pt and KEAP1. (F-G) CETSA was performed to measure the thermal stability of KEAP1 in the absence or presence of Pt at different temperatures (F) and doses (G), and the results were confirmed by WB. Data are presented as mean ± SEM. ***P* < 0.01, and ****P* < 0.001 *vs.* Ang II group in B; **P* < 0.05, ***P* < 0.01, and ****P* < 0.001 *vs.* TNF-α group in C; $^{\#\#}P$ < 0.01, and $^{\#\#\#}P$ < 0.001 *vs.* CT group in F; and ns means no significance. One-way ANOVA followed by a Bonferroni post hoc analysis for B-C, and an unpaired t-test for F.

Fig. 5. Pt diminished intracellular ROS and blocked the activation of the mtDNA-STING-TBK1 pathway. (A) Representative images of DHE staining showing increased ROS production in the aortic wall (M, media; A, adventitia) of the ApoE$^{-/-}$ mice. (B) ROS detection in RASMCs by flow cytometry following DHE staining. (C) Representative immunostaining of DNA (green) and mitochondria (Tomm20, red) showing cytosolic DNA (not localized in nuclei or mitochondria) and mtDNA in RASMCs treated with different conditions. (D) Workflow of the cytosolic dsDNA and mtDNA extraction processes. (E) A bar graph showing the quantity of cytosolic dsDNA in RASMCs treated with different conditions. (F) qPCR analysis of cytoplasmic mtDNA (*mt-Nd1* and *D-Loop*) and ribosomal gene (*18s rRNA*). (G) Immunohistochemistry assessment of STING in the suprarenal aortic walls. (H) WB analysis of the protein levels of

STING, p-STING, p-TBK1, and p-IRF3 in the aortic tissues. $^{###}P < 0.001$ *vs.* Saline group in A, G, and H; $^{*}P < 0.05$, $^{**}P < 0.01$, and $^{***}P < 0.001$ *vs.* Ang II group in A, G, and H; $^{###}P < 0.001$ *vs.* CT group in B, E, and F; $^{***}P < 0.001$ *vs.* TNF-α group in B, E, and F; and ns means no significance. One-way ANOVA followed by a Bonferroni post hoc analysis for A-B and E-H.

Fig. 6. Inhibition of the Nrf2 signaling pathway weakened the protective effect of Pt on AAA *in vitro*. RASMCs were pre-treated with 1 μM ML385 for 1 hour, then treated with Pt and positive controls for 2 hours, followed by TNF-α stimulation (10 ng/mL) for 24 hours for experiments A, B, D, E, or 6 hours for RNA isolation (C). (A) ROS detection by flow cytometry after DHE staining. (B) WB analysis of STING, p-STING, p-TBK1, and p-IRF3 in the lysates of RASMCs in indicated groups. (C) The mRNA expression levels of *Mmp2*, *Mmp3*, *Mmp9*, *Il1b*, and *Ccl2* in the different treated RASMCs as shown in the figure, with *Actb* serving as the housekeeping gene for normalization. (D) The protein expression levels of MMP2, MMP9, VCAM-1, and ICAM-1 were measured by WB analysis. (E) Protein expression (α-SMA, SM22α, and Elastin) measured by WB analysis. Data are presented as mean ± SEM. $^{*}P < 0.05$, $^{**}P < 0.01$, and $^{***}P < 0.001$; and ns means no significance. One-way ANOVA followed by a Bonferroni post hoc analysis for A-E.

Fig. 7. SMC-specific knockdown of Nrf2 abolished the protective effects of Pt on arterial wall thickness, elastic fiber degradation, and collagen deposition in the Ang II models. (A) Mouse organs in each group were extracted for fluorescence imaging. Both bright field and GFP fluorescence signals were captured under the same capture conditions. (B) Schematic illustration of the experiment design to explore the effect of Pt on SMC-specific knockdown of Nrf2 in Ang II-induced mice (n = 15 for each group). (C-D) The protein expression of Nrf2 in brain lacks SMC or in aortic media (mostly SMC). (E) Representative photographs of macroscopic features of aneurysms in the $ApoE^{-/-}$ mice. (F) The incidence rate of AAA. (G) The AAA survival curve. (H) Quantification analysis of the maximal external diameter of suprarenal aorta. (I-J) Representative images for H&E, EVG, and Masson trichrome staining of the mouse aorta, as well as elastin degradation scores. Data are presented as mean ± SEM. $^{**}P < 0.01$, and $^{***}P < 0.001$ *vs.* AAV-sh-control; $^{#}P < 0.05$, and $^{###}P < 0.001$ *vs.* Pt + AAV-sh-control; and ns means no significance. One-way ANOVA followed by a Bonferroni post hoc analysis for D, Fisher's exact test for F, Kaplan-Meier method and compared using log-rank tests for G, Brown-Forsythe ANOVA and

Welch's ANOVA test with Dunnett's T3 multiple comparison for H, non-parametric Kruskal-Wallis test followed by Dunn's post hoc analysis for J.

Fig. 8. SMC-specific knockdown of Nrf2 alleviated the anti-aneurysm effect of Pt treatment in the Ang II models. (A-B) Representative immunohistochemical staining in serial sections showing the expression of α-SMA, CD68, MMP2, MMP3, VCAM-1, and STING. (C-D) WB analysis of the protein levels of Nrf2, HO-1, MMP2, MMP9, STING, p-STING, p-TBK1, and p-IRF3 in mouse aorta samples. Adventitial tissue and endothelial tissue were removed from the aorta as much as possible. Data are presented as mean ± SEM. $^{**}P < 0.01$, and $^{***}P < 0.001$ *vs.* AAV-sh-control; $^{\#}P < 0.05$, $^{\#\#}P < 0.01$, and $^{\#\#\#}P < 0.001$ *vs.* Pt + AAV-sh-control. One-way ANOVA followed by a Bonferroni post hoc analysis for B-D.

Fig. 9. A schematic illustration showing that pterostilbene (Pt) prevented AAA formation. Under a pathological state during AAA development, Pt significantly upregulates Nrf2 and its downstream target genes (e.g., HO-1 and NQO1) by competitively binding to KEAP1 in VSMCs, thereby repressing the release of ROS. Massive ROS causes mitochondrial damage and subsequent release of mtDNA, which activates the STING-TBK1-NF-κB pathway to trigger inflammation and disrupt VSMC homeostasis (e.g., VSMC phenotype changes and matrix degradation). The ability of Pt to modulate the Nrf2 signaling pathway is responsible for the inhibition of the STING pathway and inflammatory response. Thus, targeting KEAP1-Nrf2-STING axis may be an effective strategy for AAA therapy.

Figure

Fig. 1

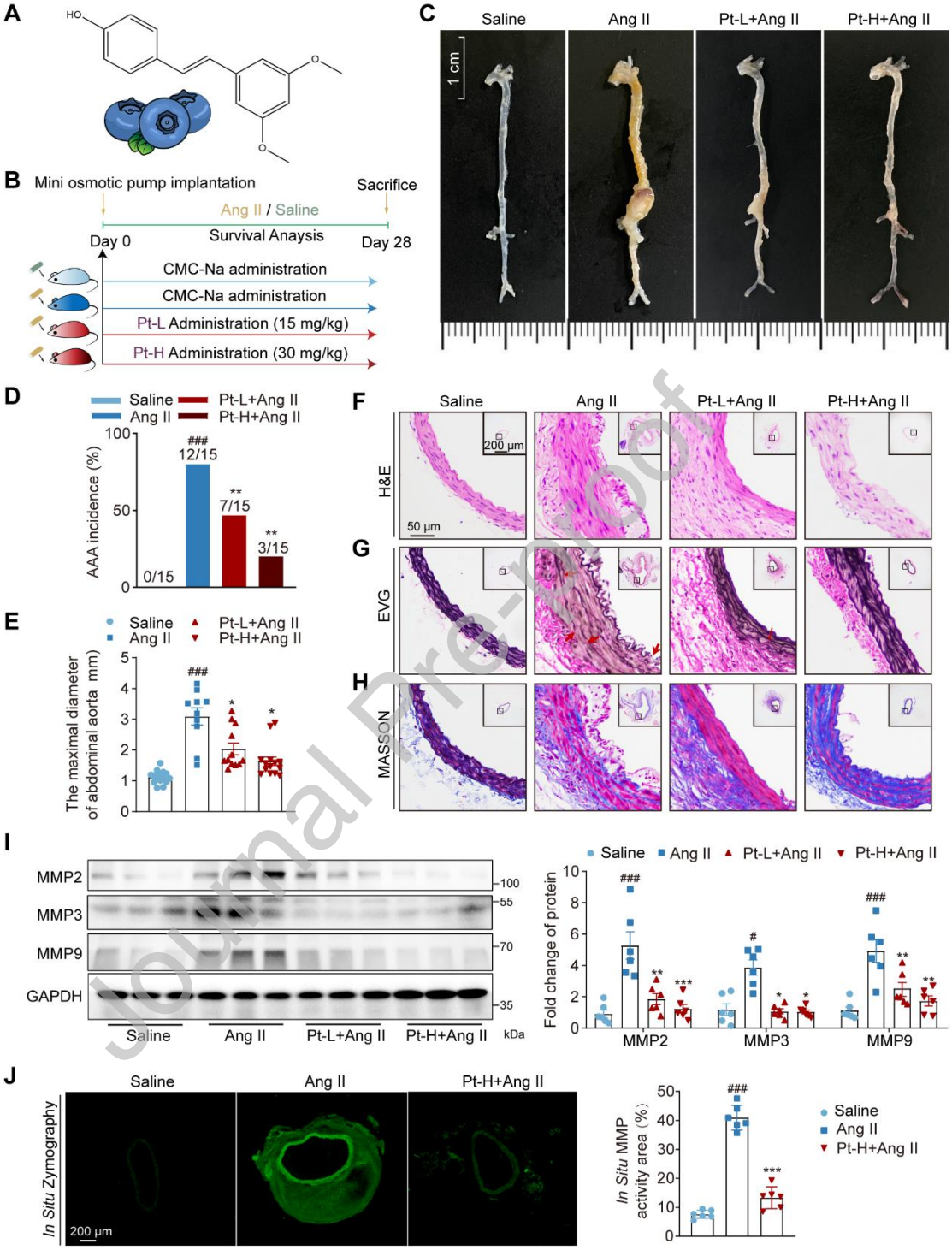

Fig. 2

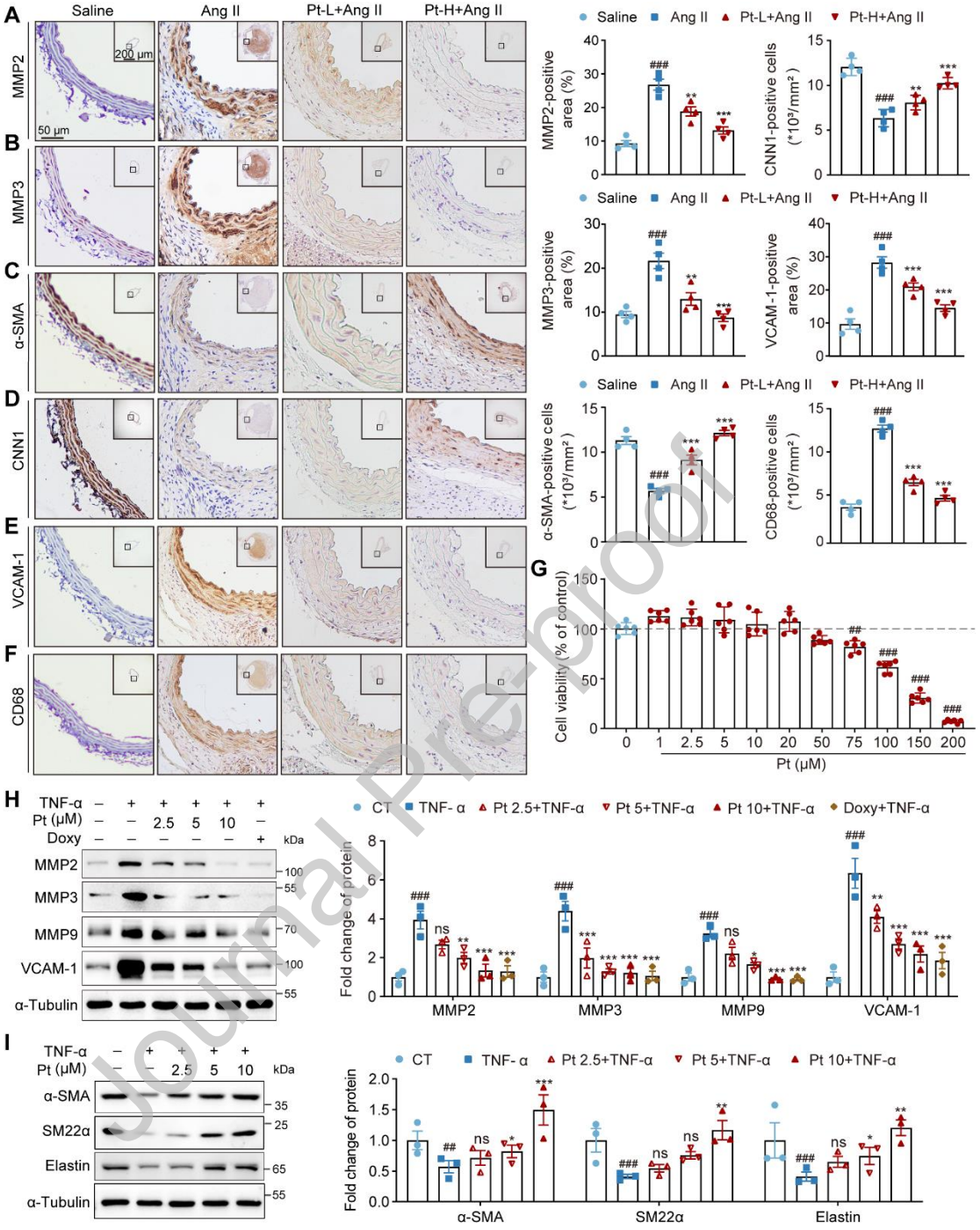

Fig. 3

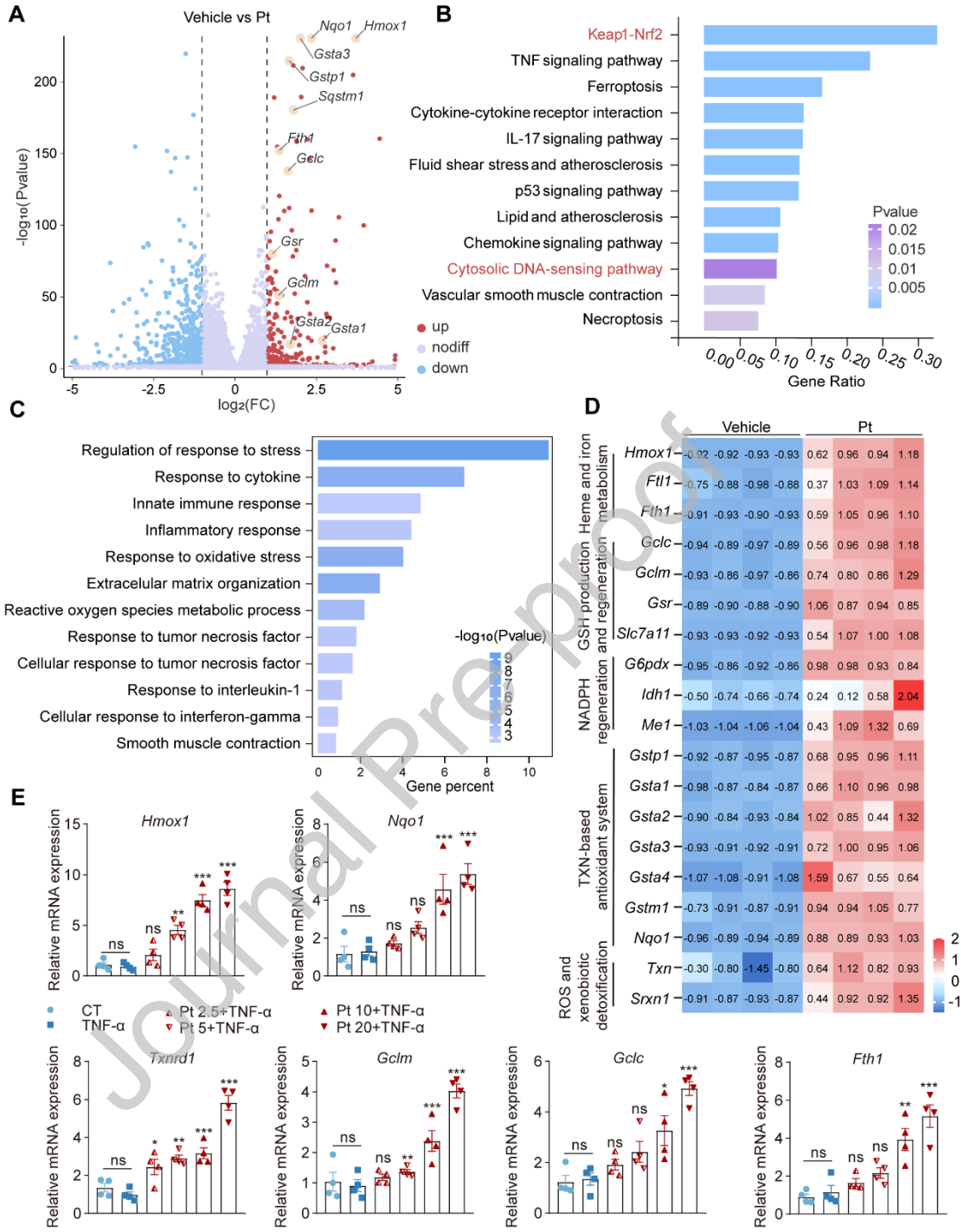

Fig. 4

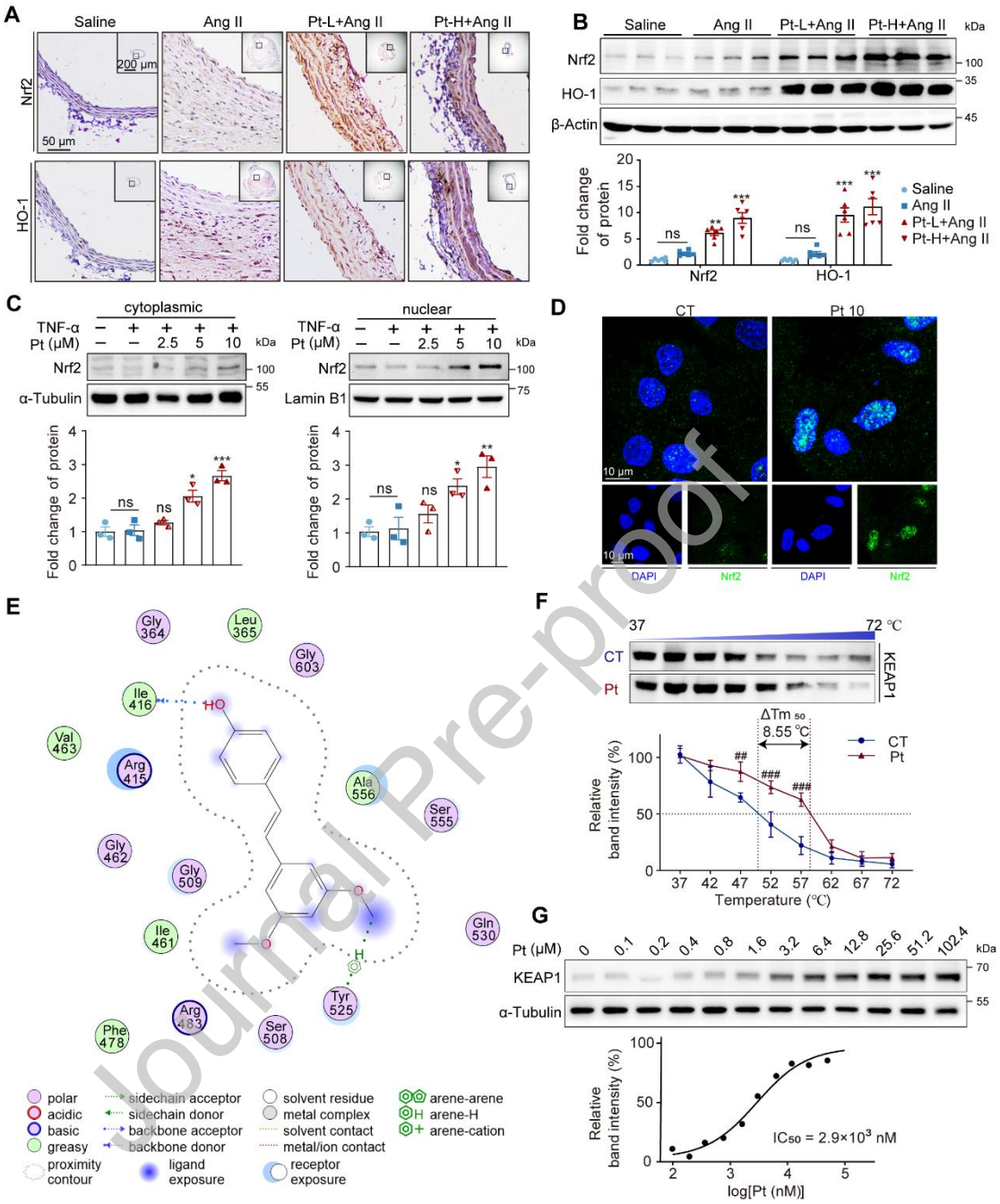

Fig. 5

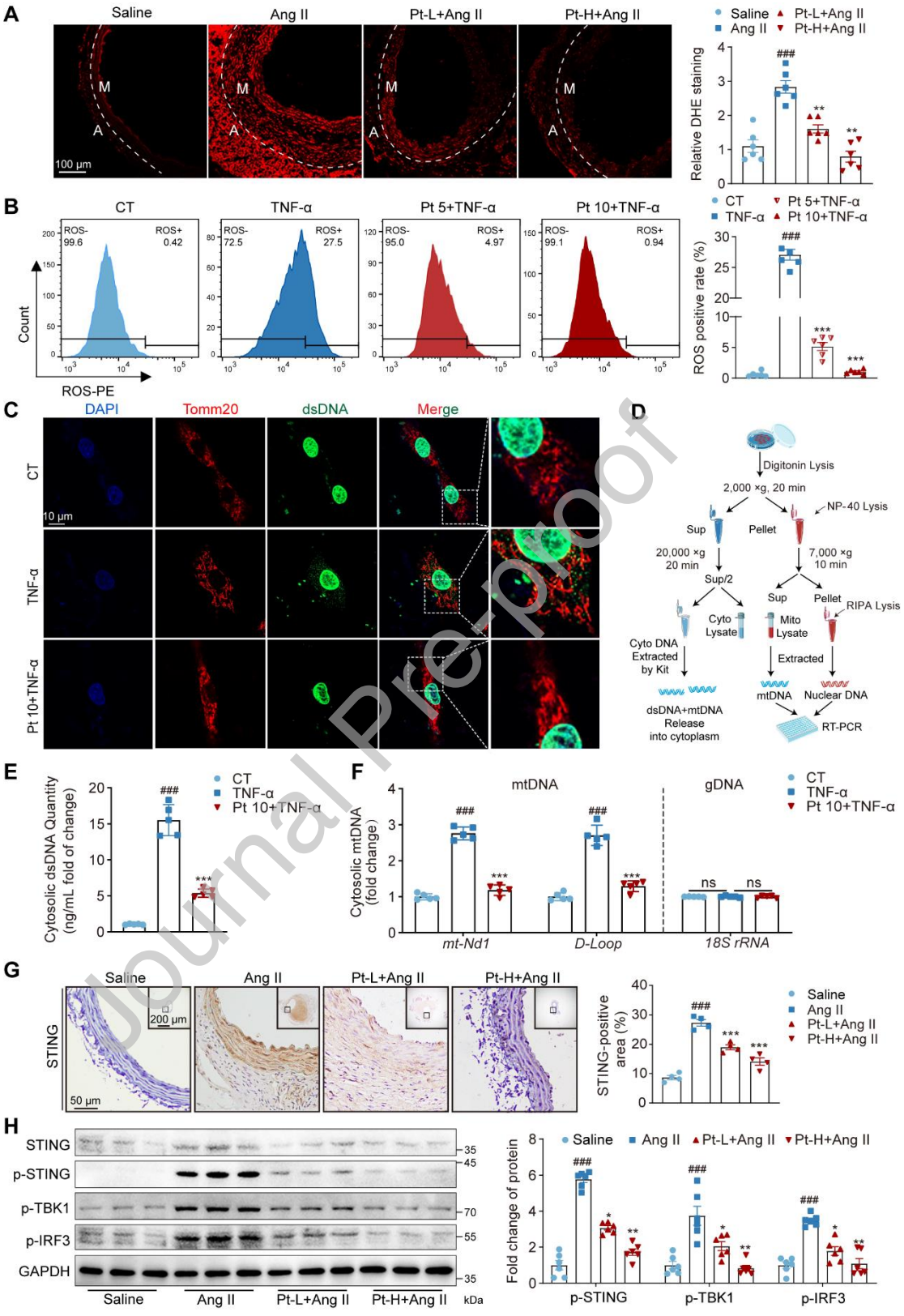

Fig. 6

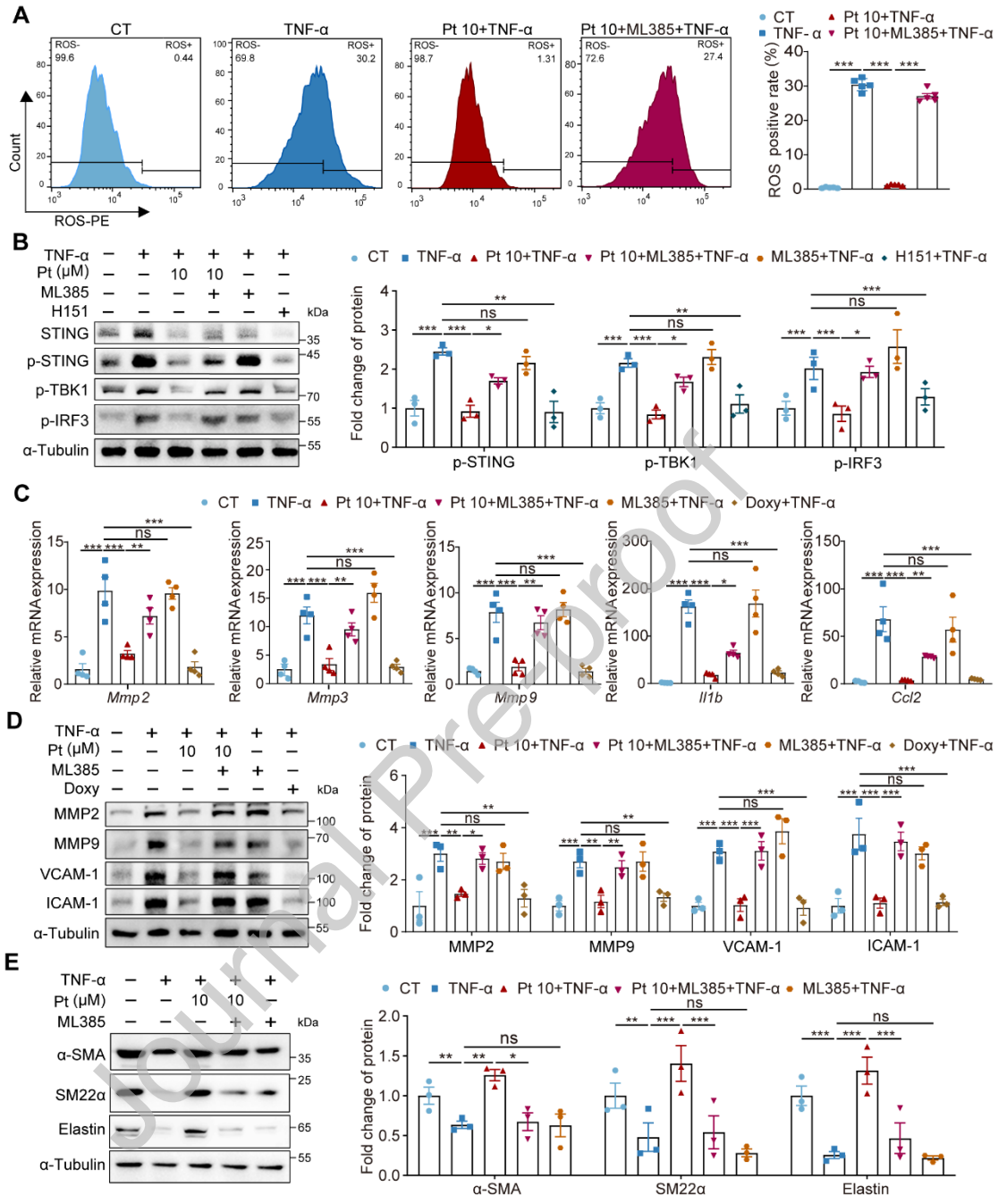

Fig. 7

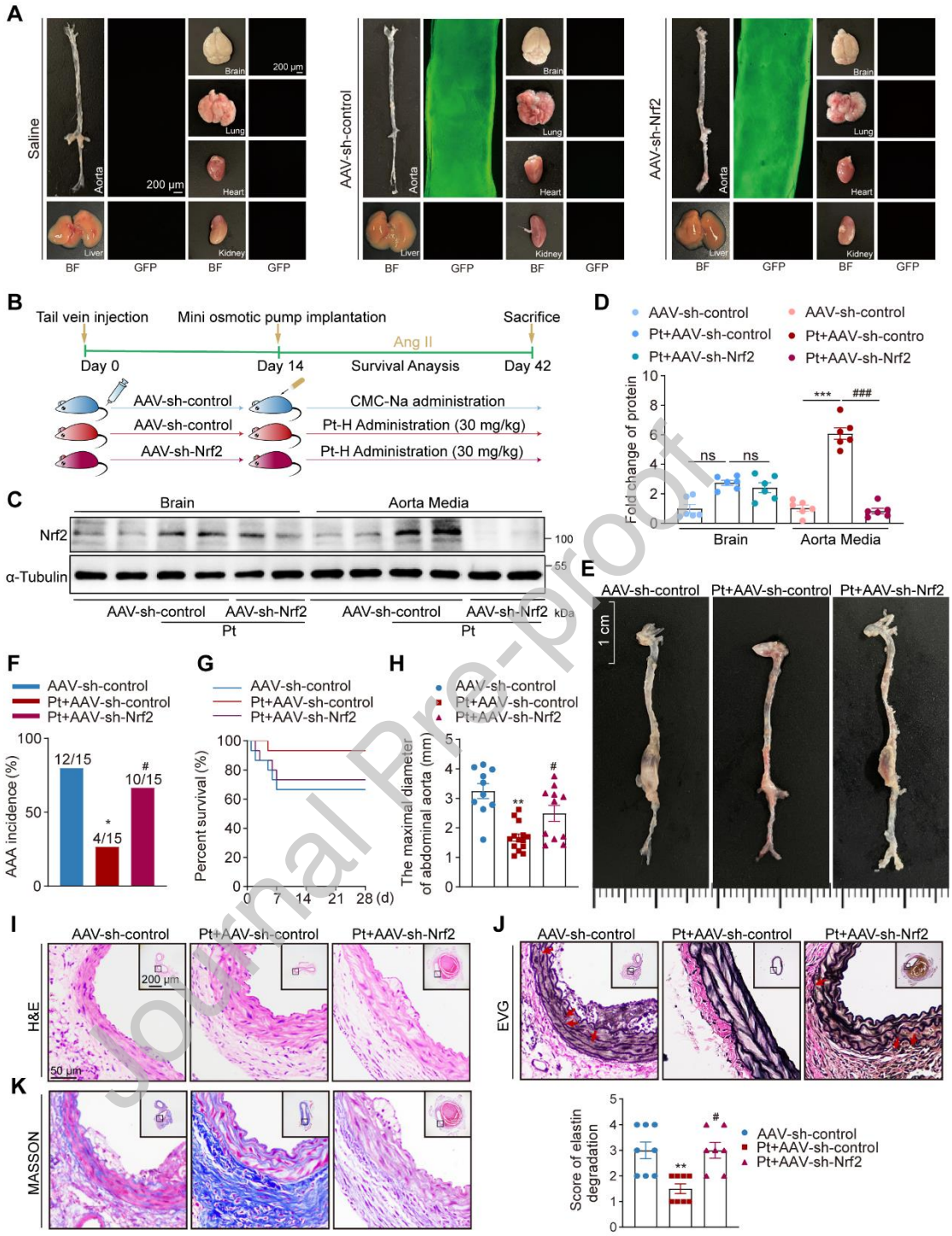

Fig. 8

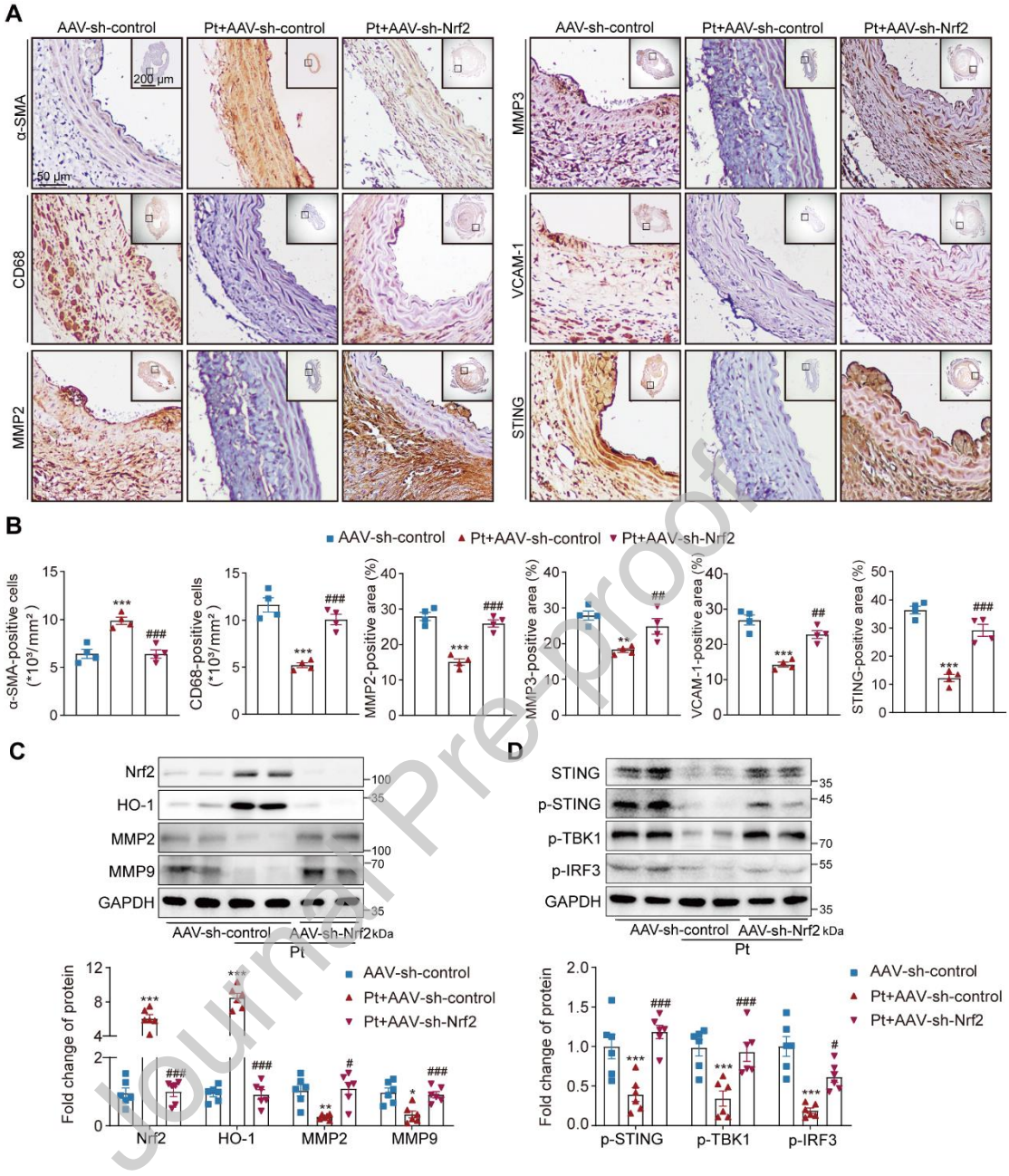

Fig. 9

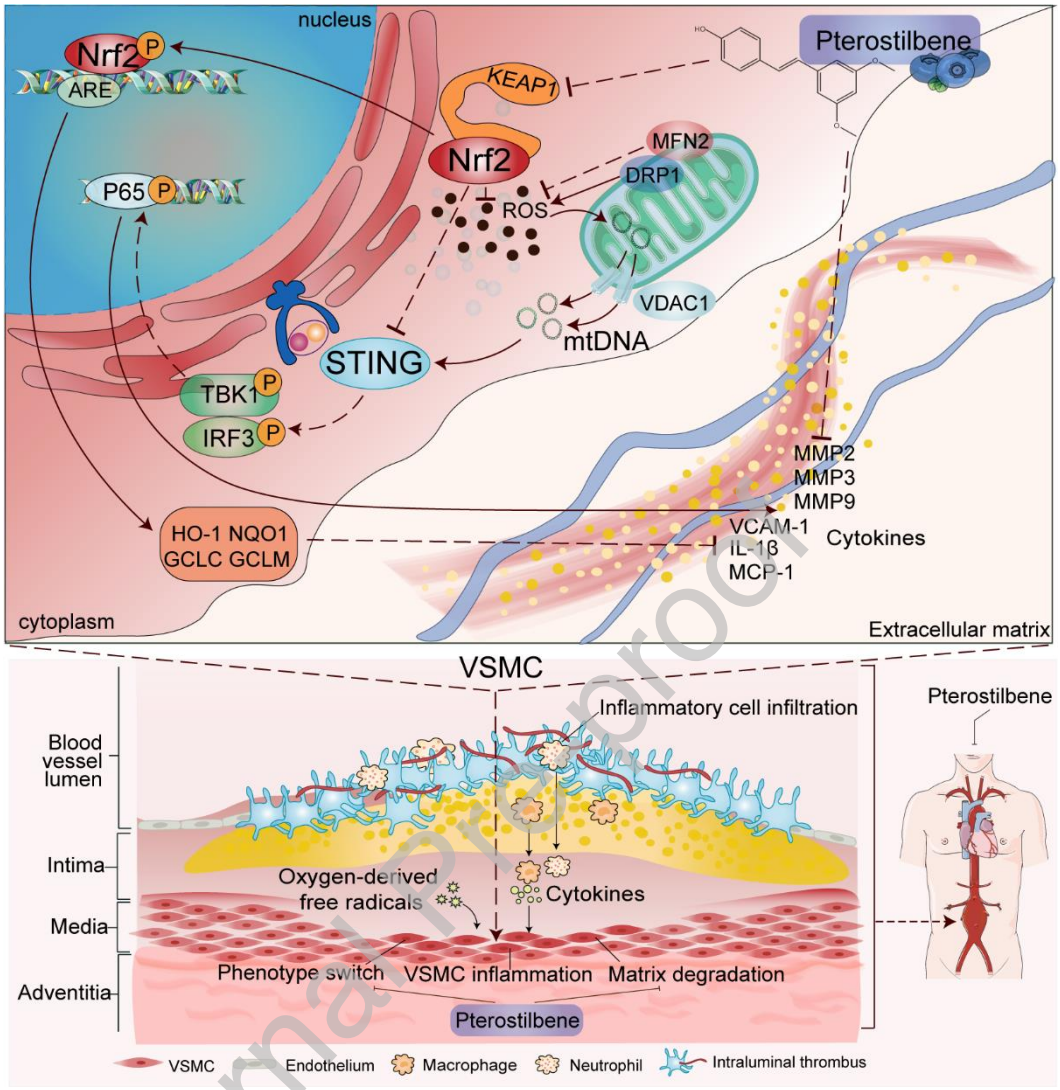

Declaration of competing interest

The authors declare that the research was conducted in the absence of any commercial or financial relationships that could be construed as a potential conflict of interest.

Graphical abstract